Contributions to Mineralogy and Petrology (2018) 173:70
https://doi.org/10.1007/s00410-018-1494-x

ORIGINAL PAPER

Near-solidus melts of MORB + 4 wt% H_2O at 0.8–2.8 GPa applied to issues of subduction magmatism and continent formation

T. W. Sisson[1] · **P. B. Kelemen**[2]

Received: 6 November 2017 / Accepted: 22 July 2018

Abstract

Experiments on MORB + 4 wt% H_2O at 0.8–2.8 GPa and 700–950 °C (Liu in High pressure phase equilibria involving the amphibolite–eclogite transformation. PhD dissertation, Stanford University, Stanford, California, 1997; Liu et al. in Earth Planet Sci Lett 143:161–171, 1996) were reexamined for their major and trace element melt compositions and melting relations. Degree of melting diminishes at greater pressures, with corresponding evolution of melt from andesitic at the lowest pressures and hottest temperatures to high-silica rhyolitic at the greatest pressure and coolest temperature. Quartz contributes greatly to the production of near-solidus melts of basaltic eclogite, with the result that melt productivity falls markedly following quartz exhaustion. This limits the extent of melting attainable in the basaltic eclogite portions of sub-arc subducting plates to no more than ~2 × the modal wt% quartz in the mafic eclogite protolith. Synthesized residual mineral assemblages lack an epidote-series mineral at temperatures > 750 °C, and as a result, melts from the rutile eclogite and rutile-amphibole eclogite facies have elevated concentrations of light rare earth elements, U, Th, have elevated Ba, K, and Sr, high Sr/Y, and are strongly depleted in Nb, Y, and the heavy rare earth elements. Models of eclogite partial melt reacting with peridotite of the mantle wedge reproduce major and trace element characteristics of parental arc magmas so long as the proportions of infiltrating melt to peridotite are relatively high, consistent with channelized ascent. Melt mass is estimated to increase roughly three- to ten-fold, consistent with H_2O concentrations of 3–7 wt% in the magmas produced by reaction. Partial melts of subducting basaltic eclogite are predicted to have positive Sr concentration anomalies, relative to Ce and Nd, that persist through melt-peridotite reactions. Primitive arc magmas commonly have positive Sr anomalies, whereas such anomalies are smaller in estimates of the bulk continental crust. Overall, Sr anomalies diminish passing from primitive to more evolved arc volcanic rocks, consistent with extensive mineral-melt differentiation (crystallization, partial remelting) involving plagioclase. On the order of 50 wt% differentiation would be necessary to eliminate Sr positive anomalies, based on geochemical variations in the Cascade and western Aleutian magmatic arcs. Loss to the mantle of cumulates and restites with high Sr anomalies, in abundances broadly equal to the mass of the preserved crust, would be required to form the continents via processes similar to present-day subduction magmatism.

Keywords Subduction magmatism · Eclogite · Partial melting · Continental crust · Experimental petrology

Introduction

Partial melting of subducting oceanic crust was proposed early in the plate tectonic revolution as a source of convergent-margin magmas (Hamilton 1969; Green and Ringwood 1966, 1968; Ringwood and Green 1966) but lost favor as trace element models indicated that eclogite facies melts of basalt would be strongly depleted in heavy rare earth elements (REE), whereas such compositions are rare in arc lavas (Gill 1974), numerical models of subduction zones predicted slab temperatures too cool for melting (Peacock 1990; Davies and Stevenson 1992), and experimental studies

Communicated by Timothy L. Grove.

Electronic supplementary material The online version of this article (https://doi.org/10.1007/s00410-018-1494-x) contains supplementary material, which is available to authorized users.

✉ T. W. Sisson
tsisson@usgs.gov

[1] U.S. Geological Survey, 345 Middlefield Road, Menlo Park, CA 94025, USA

[2] Lamont-Doherty Earth Observatory, Columbia University, New York, USA

Published online: 11 August 2018

showed that amphibole, the major carrier of H_2O in the crustal portion of subducting oceanic lithosphere, would have reacted out before slabs reached sub-arc depths (Wyllie 1973).

However, more recent dynamic models (Furukawa 1993; van Keken et al. 2002; Kelemen et al. 2003b; Peacock et al. 2005; Wada and Wang 2009; Syracuse et al. 2010), predict sub-arc slab-surface temperatures reaching or exceeding the solidus of wet phengite-bearing basaltic eclogite (Schmidt and Poli 1998; Poli and Schmidt 2002) for about half of the world's subduction zones. Robust pressure–temperature estimates for high-pressure and ultra-high-pressure eclogites cluster close to the wet solidus, possibly due to higher temperature rocks having partly melted and disaggregated, or due to reactions having arrested as partly molten rocks cooled across the solidus (Hacker 2006; Penniston-Dorland et al. 2015).

Thermochemical modeling of arc magma generation (Hermann and Rubatto 2009; Plank et al. 2009; Cooper et al. 2012) is also consistent with slab-surface temperatures commonly exceeding the wet solidi of basalt and sediment by small amounts or attaining temperatures sufficient to produce melt-like supercritical fluid. Serpentine and chlorite are now known to be stable to sub-arc depths in subducting ultramafic rocks where they may then break down (Ulmer and Trommsdorff 1995; Grove et al. 2006; Till et al. 2012), reviving and refining scenarios (Ringwood 1977) wherein hydrated portions of the subducting mantle lithosphere release H_2O beneath arcs, triggering melting in superjacent slab eclogite. Thus, a door has reopened to the likelihood that slab partial melting contributes to present-day subduction magmatism, but it is unclear if such melting is rare or widespread.

High-quality experiments are a powerful approach for understanding subduction magmatism, but shortcomings remain in some conditions employed to investigate the possible partial melting of subducting basaltic crust. Sub-solidus phase relations are well-established for basalt + H_2O, as is the location of the basalt + H_2O ± phengite solidus (Schmidt and Poli 1998; Schmidt et al. 2004). Dehydration melting of mafic amphibolites was studied comprehensively at 0.8–3.2 GPa and ≥ 1000 °C (Rapp et al. 1991; Rapp and Watson 1995), considerably hotter than numerical simulations and geochemical models predict for slabs passing beneath active magmatic arcs. Similarly, Klemme et al. (2002) studied an Fe-free synthetic eclogite at 1200–1400 °C and 3 GPa, well above the *T*/*P* estimated for most subduction zones. Klimm et al. (2008) and Kessel et al. (2005a, b) studied phase relations of basaltic compositions at pressure–temperature conditions overlapping those modeled for subducting oceanic crust (750–900 °C at 2.5 GPa; 700–1400 °C at 4, 5, and 6 GPa, respectively). However, to facilitate the production and analysis of fluid or melt, those studies employed high concentrations of H_2O (19–21 wt%; 8–24 wt%, respectively), which enhances melting.

To add to these and other prior results, we report herein a project of opportunity, reanalyzing and reinterpreting supersolidus phase equilibrium runs on a fresh mid-ocean ridge basalt (MORB) glass + 4 wt% H_2O at 800, 900, and 950 °C and 0.8–2.8 GPa mostly produced in the PhD project of Liu (1997), partly reported in Liu et al. (1996) and Ernst and Liu (1998). Those papers emphasize mineral stability relations and compositions in subducting mafic oceanic crust, but many runs crossed the H_2O-saturated solidus and fill a low-temperature hole in the available experimental data, closer to conditions anticipated for slab melting. We apply those atypically long-duration oxygen-buffered experimental results to explore various aspects and scenarios of magma generation in subduction zones.

Sample and experimental methods

Liu (1997) performed piston-cylinder experiments at the USGS Menlo Park, California, at 0.8–3.0 GPa and 600–950 °C on a powdered fresh MORB glass plus 4 wt% added H_2O, with fO_2 buffered at quartz + fayalite + magnetite or quartz + ferrosilite + magnetite. Those experiments were conducted to investigate subsolidus mineral and mineral-fluid stability relations in subducting basaltic crust, but runs quenched from hotter than 700 °C were identified as containing glass (reexamination in this study identifies glass in some products from 700 °C), and the glass is sufficiently abundant to analyze by electron-microprobe in runs performed at 800 °C and hotter. The basalt was reported to be from the Juan de Fuca (JDF) spreading ridge (Liu et al. 1996; Ernst and Liu 1998) but its identifying sample number has been lost. Electron microprobe analysis of the glass (Table 1) and referencing the Smithsonian Abyssal Volcanic Glass Database (https://mineralsciences.si.edu/research/glass/vg.htm) establishes it as similar to glasses recovered by dredge 10 of the 1968 RV Oceanographer cruise to the southern medial valley of the Juan de Fuca ridge. The glass contains a few percent of olivine and acicular plagioclase microphenocrysts, and it lacks hydration or secondary minerals. Splits of the bulk JDF MORB sample were analyzed for major and trace elements in the laboratories of the USGS, Denver, Colorado, and the Geoanalytical Laboratory at Washington State University, Pullman, Washington (Table 1). Transmission FTIR of the natural glass using the 3570 cm^{-1} absorption indicates dissolved H_2O of 0.3 wt% (D. Blatter, written communication).

Liu's (1997) experiments were performed in end-loaded piston-cylinder presses using NaCl and NaCl-Pyrex assemblies (2.54 cm diameter vessels to 2.0 GPa, and 1.91 cm diameter > 2.0 GPa), with pressure calibrated by bracketing

Table 1 Chemical composition of JDF pillow basalt rind

	WR WSU	WR USGS	Emp glass
SiO_2 (wt%)	50.29	50.70	50.57
TiO_2	1.96	1.96	1.91
Al_2O_3	14.04	14.10	14.21
FeOt	12.51	12.40	12.26
MnO	0.22	0.22	0.21
MgO	6.90	6.92	6.64
CaO	11.09	11.10	11.03
Na_2O	2.63	2.53	2.60
K_2O	0.17	0.17	0.19
P_2O_5	0.18	0.20	0.21
Cl	–	–	0.04
SO_3	–	–	0.32
Total	99.99	100.30	100.18
	XRF	XRF	
Rb (ppm)	4	3	–
Sr	95	97	–
Ba	30	31	–
Y	43	46	–
Zr	117	129	–
Nb	4.7	< 10	–
V	369	392	–
Cu	58	56	–
Ni	67	65	–
Zn	104	103	–
Cr	167	–	–
Sc	45	–	–
	ICPMS	INAA	
Cs (ppm)	0.03	–	–
Rb	2.3	–	–
Sr	98	–	–
Ba	25	–	–
Y	44.6	–	–
Zr	124	–	–
Hf	3.39	3.57	–
Nb	4.79	–	–
Ta	0.49	0.38	–
Th	0.42	–	–
U	0.16	–	–
Pb	0.65	–	–
La	5.31	5.39	–
Ce	14.78	17.1	–
Pr	2.46	–	–
Nd	12.85	14.1	–
Sm	4.62	5.01	–
Eu	1.67	1.65	–
Gd	6.66	6.16	–
Tb	1.22	1.16	–
Dy	8.41	–	–
Ho	1.78	–	–
Er	4.93	–	–
Tm	0.73	0.83	–
Yb	4.51	5.18	–
Lu	0.71	0.75	–
Sc	43.3	46.8	–
Cr	–	186	–
Co	–	47	–

Emp averages 116 electron microprobe analyses of glass, WR is whole rock including minor microphenocrysts; INAA reported only for elements with counting uncertainties < 5% relative; FeOt, all Fe as FeO; –, not analyzed or not reported due to low precision; FTIR on glass gives 0.3 wt% H_2O

the albite = jadeite + quartz (Liu and Bohlen 1995) and quartz = coesite reactions (Bohlen and Boettcher 1982). Powdered glass (20–25 mg) plus ~ 4 wt% H_2O were weighed into 3 mm O.D. $Ag_{70}Pd_{30}$ capsules and sealed by arc welding with the capsule protruding into an ice-water bath to inhibit H_2O evaporation. Sealed sample capsules were then centered into 5 mm O.D. Au outer capsules packed with powdered quartz + fayalite + magnetite + H_2O and sealed by arc welding. Possible sluggish nucleation of garnet was addressed by adding a trace of natural almandine to selected runs and by re-running at garnet-free conditions some experiments that previously grew garnet. Run durations generally varied inversely with temperature, with sub-solidus runs as long as 90 days (successive 45 day runs with reloaded buffer capsules), 800 °C runs of 5–25.5 days, 900 °C runs of 3–12.5 days, and 950 °C runs of 4–8 days. Runs that could be located, and with sufficient melt for analysis, are reported in Table 2 and include additional super-solidus experiments at 2.6 and 2.8 GPa and 800 and 900 °C conducted during the present study to better replicate slab partial-melting conditions. The new experiments used the same MORB sample, capsule, and buffer materials, and similar methods as in the previous work, except for greater sample amounts (40 mg). New runs at 800 °C were duplicated to investigate reproducibility of results. The new 800 °C runs produced a silica mineral whose identity as quartz was verified by re-bracketing the quartz = coesite reaction. Liu (1997) and we verified the presence of H_2O in the outer capsules of quenched runs by the weigh-puncture-heat-reweigh method, and survival of the buffer assemblage by X-ray diffraction (ferrosilite + quartz + magnetite above 1.1–1.2 GPa at 800–900 °C). Insofar as possible, the original epoxy-mounted samples of Liu (1997) were repolished and reexamined by electron-microprobe methods, but some original sample mounts could not be found, and missing

Table 2 Synthesis conditions and phase abundances of 800, 900, and 950 °C runs on JDF MORB + H_2O

Run	Conditions				Phase proportions (wt%)										Bubbles[a]
	GPa	°C	hours	+H_2O wt%	Melt + fluid	qtz	plag	amph	cpx	gt	ilm	rut	tit	ap	
99	1.0	800	288	4.4	29.6	0	<<1[d]	55.1	11.1	3.0	0	0	1.1	0.3	Y
70	1.2	800	241	3.8	25.4	0	< 1	56.8	12.0	3.5	0	0	1.8	0.4	Y, P
71[b]	1.4	800	261	4.0	16.6	4.7	0	56.2	15.8	4.7	0	0	1.6	0.4	Y, P
73	1.6	800	283	4.2	25.0	0	0	24.9	25.3	23.7	0	1.1	0	0.4	Y, P
75	1.8	800	217	3.4	21.6	0	0	25.4	27.9	24.2	0	1.1	0	0.4	Y, P
146	2.0	800	310	4.2	22.2	0	0	0	37.0	39.6	0	1.2	0	0.4	P
120	2.2	800	121	4.0	21.8	0	0	0	36.9	40.0	0	1.3	0	0.4	P
2242	2.6	800	240	4.0	18.7	1.8	0	0	37.1	41.0	0	1.1	0	0.4	q
2237	2.6	800	216	4.0	19.1	0.4	0	0	40.0	39.2	0	1.2	0	0.4	q
2241	2.8	800	240	4.0	17.1	1.3	0	0	41.7	38.7	0	1.2	0	0.4	q
2238	2.8	800	218	4.0	14.4	3.6	0	0	39.3	41.3	0	1.2	0	0.4	q
2238[c]	2.8	800	218	4.0	16.0	2.4	0	0	40.2	40.0	0	1.2	0	0.4	q
53	0.8	900	99	4.0	34.8	0	< 1	46.5	17.9	0	0.9	0	0	0.1	Y
55	1.0	900	95	4.0	33.6	0	< 1	41.6	23.8	0	1.2	0	0	0.1	Y
57	1.2	900	93	3.8	32.6	0	0	27.9	30.8	7.6	1.6	0	0	0.1	q
59	1.4	900	73	3.9	29.1	0	0	< 1	40.3	29.7	0	1.0	0	0.3	Y, P
61	1.6	900	91	3.9	26.8	0	0	0	42.2	30.1	0	1.0	0	0.4	Y
64	1.8	900	120	4.1	27.5	0	0	0	35.1	35.8	0	1.1	0	0.3	q
2256	2.6	900	240	4.0	22.3	0	0	0	35.7	40.6	0	1.2	0	0.3	q
2255	2.8	900	240	4.0	21.2	0	0	0	35.6	42.4	0	0.9	0	0.4	q
112	1.1	950	144	4.0	40.6	0	0	21.1	31.5	5.8	1.6	0	0	0	Y
103	1.2	950	94	3.9	38.7	0	0	< 1	39.4	20.0	2.8	0	0	0	Y
105	1.4	950	118	4.1	34.8	0	0	0	39.2	24.0	2.6	0	0	0	Y

qtz quartz, *plag* plagioclase, *amph* amphibole, *cpx* clinopyroxene, *gt* garnet, *ilm* ilmenite, *rut* rutile, *tit* titanite, *ap* apatite

[a] *Y* yes, some spherical bubbles > 10 mm, *P* open angular pores bounded by mineral grains, *q* small spherical bubbles (< 5 mm) along edges of mineral grains and in centers of glass pools interpreted as quench vesicles

[b] Possibly run 72 with $H_2O + CO_2$, see text

[c] Results for run 2238 using 2241 pyroxene

[d] Liu (1997) found plagioclase in this run but we did not

samples were remounted from labeled vials of excess run products, as were the new 2.6 and 2.8 GPa runs. Runs at 700 and 750 °C were also reexamined (Table 3), resulting in slight revisions to the phase assemblages reported by Liu (1997) and Liu et al. (1996), notably the presence of a stable field of clinozoisite or zoisite, and the aforementioned identification of traces of glass in some of the 700 °C runs.

Analytical methods

Liu (1997) reports major oxide compositions of synthesized minerals and of 900 and 950 °C glasses analyzed with wavelength dispersive techniques on the USGS 5-spectrometer JEOL8900R electron microprobe, with conditions of 15 kV accelerating potential, 15 nA Faraday current, and a focused beam for minerals and a 5 µm diameter beam for glass. Low Na_2O concentrations reported for glasses signaled inappropriately high current densities during analysis, leading to Na migration (Morgan and London 1996). Accordingly, glasses in 800, 900, and 950 °C runs were analyzed or re-analyzed with the USGS electron microprobe at 15 kV with a 2 nA Faraday current, 10–15 µm beam diameter, and Na measured first for 5 s. Ratajeski (1999) showed these methods successfully mitigate Na migration in rhyolite glass with up to 5 wt% dissolved H_2O. Background-corrected X-ray intensities were reduced to concentrations with the JEOL version of the CITZAF routine (Armstrong 1995). Composite mineral + glass analyses were identified by their outlier compositions and rejected, and averages of the remaining glass analyses are reported in Supplemental Table 1 (ST-1). Although glass can be distinguished in some of the 700 °C runs, and in all 750 °C runs, it proved too finely distributed between crystals for accurate analyses and compositions are not reported.

Table 3 Synthesis conditions and phases identified in selected 700 and 750 °C runs on JDF MORB + H_2O

run	Conditions				Phases identified											
	GPa	°C	hours	H_2O wt%	fluid	glass	qtz	coe	plag	amph	cpx	gt	ilm	rut	tit	czo	Other
101	0.8	700	669	4.0	Y	Y			Y	Y					Y		sulf, gt-seeds
97	1.0	700	573	3.9	Y		Y		Y	Y					Y		
131	1.2	700	500	4.2	Y	Y	Y		Y	Y	Y	Y			Y	Y	
185	1.4	700	774	4.1	Y		Y			Y		Y			Y	Y	zirc
188	1.6	700	720	4.1	Y		Y			Y		Y			Y	Y	
189	1.6	700	720	10.7	Y	Y	Y			Y	Y	Y			Y	Y[a]	
160	1.8	700	549	4.0	Y		Y			Y	Y	Y		Y		Y[a]	
184	1.8	700	1101	3.7	Y		Y			Y	Y	Y		Y			
125	2.2	700	284	3.9	Y	Y	Y				Y	Y		Y			
128	2.6	700	161	4.1	Y		Y				Y	Y		Y			pheng, staurl
182	3.0	700	406	4.0	Y			Y			Y	Y		Y			zirc, ky
133	1.2	750	336	4.1	Y	Y			Y	Y		Y			Y	Y	
144	2.2	750	596	4.1	Y	Y					Y	Y		Y			zirc, sulf

qtz quartz, *coe* coesite, *plag* plagioclase, *amph* amphibole, *cpx* clinopyroxene, *gt* garnet, *ilm* ilmenite, *rut* rutile, *tit* titanite, *czo* clinozoisite, *sulf* Fe-sulfide, *zirc* zircon, *pheng* phengite, *staurl* staurolite, *ky* kyanite

[a]Run was seeded with clinozoisite

Synthesized minerals were analyzed in the new 2.6 and 2.8 GPa runs and in some runs from Liu (1997) if initial attempts to estimate phase proportions by mass-balance yielded poor residuals, if mineral–mineral or mineral-melt exchange K_Ds had anomalous values, or where a phase had been overlooked. Minerals were analyzed with a focused 15 kV beam at 15 or 20 nA Faraday current, except for plagioclase, which was analyzed with a 2 µm beam diameter and 8 nA Faraday current. Where sufficiently coarse (e.g., garnet), mineral rims were analyzed preferentially to obtain compositions that approach exchange equilibrium with melt and other phases. Garnet grains have slight rimward enrichments in Mg/Fe visible in backscattered X-ray images; no other minerals have discernable consistent differences between rims and interiors. Composite mineral + glass analyses were identified by anomalously high SiO_2, Na_2O, and K_2O concentrations and rejected, and averages of the remaining analyses are reported in ST-2 along with their sources (this study; Liu 1997). Entries for FeOt and MgO, and for Fe and Mg, were transposed for clinopyroxene in the data tables of Liu (1997), and these typographic errors are corrected herein.

Trace element concentrations of selected glasses were analyzed by ion microprobe at the Woods Hole Oceanographic Institute (WHOI) and at the Stanford-USGS SHRIMP facility. Because the runs were not designed to segregate melt and thereby facilitate its trace element analysis, it proved difficult to avoid composite analyses of glass and crystals, so acceptable trace element results are few and are presented as reconnaissance values. Analyses at WHOI employed the CAMECA IMS-3f instrument using energy filtering (reduced secondary accelerating voltage) to suppress molecular-ion interferences (Shimizu and Hart 1982), whereas the Stanford-USGS SHRIMP instrument relies on high mass-resolution to separate intended from interfering peaks. Both instruments employed an oxygen primary beam focused to spot sizes of approximately 10 µm and were standardized on a suite of natural rhyolite obsidian glasses (Macdonald et al. 1992), using linear working curves with zero intercepts to convert ion intensity ratios to weight concentrations. Mg, P, Ca, Al, and Ti were monitored to identify beam overlap onto crystals, and points with anomalously high count-rates for one or more of those elements were rejected. Supplemental Table 3 reports averages of accepted trace element analyses of synthesized glasses and of the obsidian standards measured as unknowns.

Mass-balance estimates of phase proportions and of reconstructed melt (± fluid) compositions

Weight proportions of synthesized phases (Table 2) were estimated by linear least squares multiple regression matching the sample's major oxide composition, including added and original H_2O, with those of the analyzed phases. Nominally anhydrous minerals were normalized to 100 wt%, anhydrous, whereas amphibole compositions were normalized to 98.25 wt% and were assigned 1.75 wt% H_2O, as is typical for igneous amphiboles (Dodge et al. 1968). Most of the quenched glasses contain bubbles (Table 2), but it is unclear which resulted from a fluid phase stable at run

conditions[1], and which formed or expanded due to pressure reduction during quenching (Bista et al. 2015). To account for H_2O in bubbles, glass compositions were normalized anhydrous, and pure H_2O was included in mass-balance regressions as a separate phase, potentially fictive. Negative residuals for Na_2O in an initial round of mass-balance results signaled Na-loss from glass during analysis, that significant Na was hosted in a high-pressure fluid phase, or both. Least-squares calculations were, therefore, repeated including pure Na_2O as a fictive phase, and the anhydrous-normalized glass, H_2O, and fictive Na_2O phase were combined in their respective proportions to reconstruct the composition of melt (± fluid) (ST-4). Because the runs are mineral-rich, reconstructed melt (± fluid) compositions and phase proportions are sensitive to average mineral compositions. To investigate this, phase proportions for run 2238 at 2.8 GPa and 800 °C were also estimated by mass-balance substituting the slightly more sodic pyroxene of run 2241 produced under the same *P*–*T* conditions. Derived phase proportions are similar (Table 2), but the calculated melt (± fluid) fraction is slightly greater and less sodic (ST-4). The proportion of apatite estimated by least squares varied erratically, probably controlled by the Ca budget of the assemblage, therefore, apatite abundances were recalculated from P_2O_5 residuals.

Results

Mineral assemblages and compositions

Except for a stable field of clinozoisite (or zoisite) extending to slightly more than 750 °C (Table 3; Fig. 1), no important differences were found in the mineral stability limits from those reported by Liu et al. (1996) and Liu (1997). Supersolidus mineral assemblages are dominated by amphibole, clinopyroxene, and garnet, accompanied by ilmenite, titanite, or rutile (Fig. 2). At pressures greater than the amphibole-out boundary, supersolidus mineral assemblages consist of sub-equal amounts of garnet and clinopyroxene (i.e., eclogite) with accessory rutile, and a field of rutile–quartz eclogite at 800 °C and 2.6 and 2.8 GPa. Pyroxenes are richer in Na in higher-pressure supersolidus runs: for 800 or 900 °C ranging from aluminous diopside at 1.0 or 1.2 GPa, through aluminous sodic diopside or augite, to omphacite at greater than 1.8 GPa (Morimoto 1988). Garnets consist dominantly of almandine (Fe/Fe + Mg + Ca: 0.53–0.45)

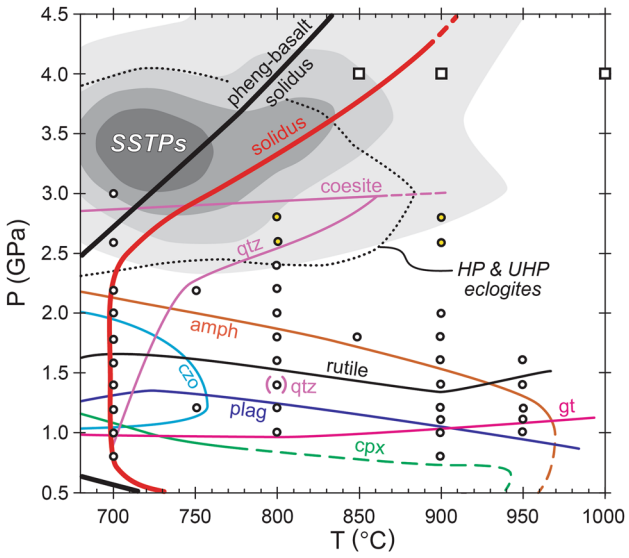

Fig. 1 Phase stability limits for JDF MORB + 4 wt% H_2O at fO_2 = quartz–fayalite–magnetite and quartz–ferrosilite–magnetite; mineral names lie on stable side of appearance boundaries; stability limits are dashed where not bracketed. Open circles: runs from Liu et al. (1996), Liu (1997), and this study (Tables 2, 3); squares: runs from Kessel et al. (2005b) that locate the 4.0 GPa K-free haplobasalt + H_2O solidus. Heavy black line: H_2O + phengite saturated basalt solidus from Schmidt and Poli (1998). The solidus for JDF MORB + 4 wt% H_2O (thick red line) is drawn isothermal at 700 °C from 0.8 to 2.2 GPa to account for sporadic appearance of glass at that temperature and is dashed at greater than 4 GPa due to the uncertain conditions of the second critical endpoint. Shaded field encompasses sub-arc slab surface temperatures and pressures (*SSTPs*) from subduction zone numerical simulations of Wada and Wang (2009) and Syracuse et al. (2010) (80 km coupling model D80), with more abundant solutions in darker shading (shadings in this and subsequent figures are calculated with the kernel density tool of ArcMap). Dotted black line labeled HP & UHP eclogites encloses pressure–temperature solutions for kyanite plus phengite bearing eclogites from Hacker (2006). Stability of quartz in the run at 1.4 GPa and 800 °C is considered suspect and may be due to misidentification of run mounts, as discussed in text

with subordinate grossular (Ca/Fe + Mg + Ca: 0.36–0.22) and pyrope (Mg/Fe + Mg + Ca: 0.16–0.32). The chief variation in garnet composition is an increasing proportion of pyrope, a decreasing proportion of grossular, and a slightly diminishing proportion of almandine, with increasing pressure and temperature, which corresponds with diminishing abundance of amphibole. Garnets grown at 800 and 900 °C plot in the field of group C (blueschist associated) eclogite garnets (Coleman et al. 1965), but they trend with increasing pressure and temperature to the field of group B (migmatitic gneiss) eclogite garnets, where the 950 °C garnets plot. The array of compositions is also similar to garnets from amphibolites, charnockites, and granulites (Coleman et al. 1965).

Amphibole is the most abundant mineral at the lowest pressures investigated, where the residual assemblages would be classified as garnet–pyroxene hornblendite (or

[1] Experience in the USGS lab is for dissolved CO_2 of 1000–2000 ppm in melts produced in piston-cylinder experiments, leading to bubbles at pressures greater than for saturation with pure-H_2O fluids.

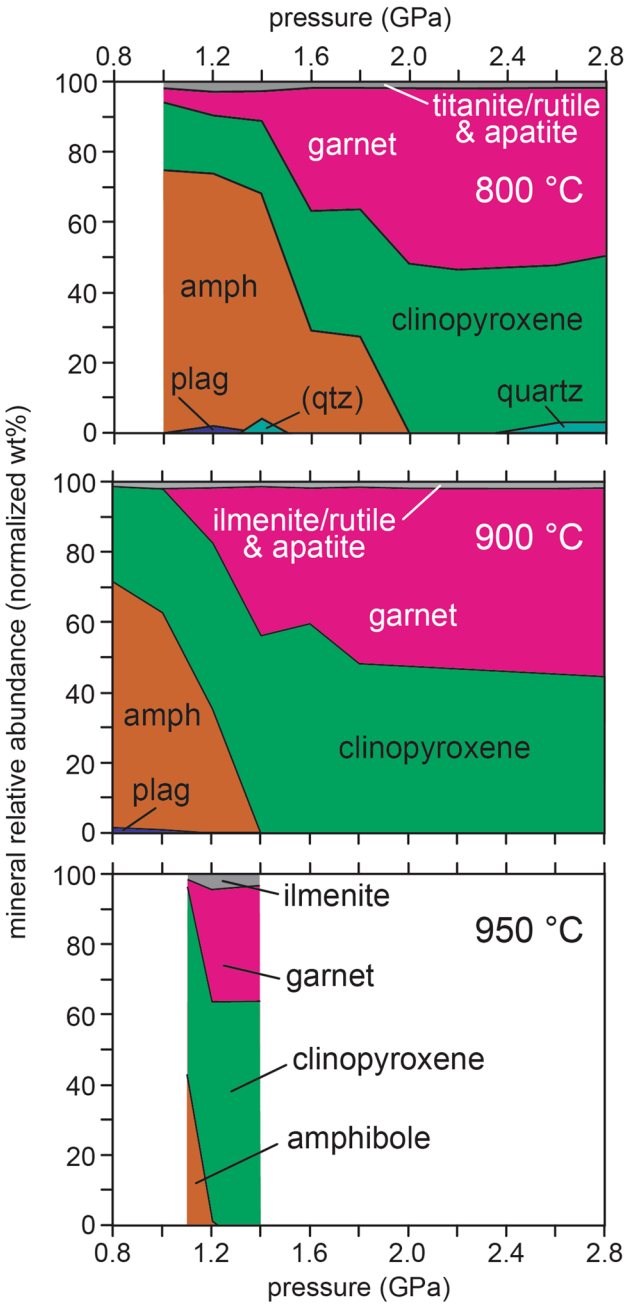

Fig. 2 Relative abundances of minerals synthesized at 800, 900, and 950 °C from JDF MORB + 4 wt% H_2O, expressed in weight percent, normalized melt- and fluid-free (Table 2). Isolated appearance of quartz at 1.4 GPa and 800 °C is considered suspect and may be due to misidentification of run mounts, as discussed in text

garnet-pyroxene amphibolite) at 800 °C, pyroxene hornblendite at 900 °C, and hornblende clinopyroxenite at 950 °C. Plagioclase is present only in the lower pressure run products and only in trace amounts. Plagioclase analyzed in run 70 (800 °C, 1.2 GPa) cluster in two compositional groups, but the significance is unknown due to their scarcity and fine grain size. Amphibole abundance diminishes with increasing pressure antithetic to the increasing abundance of garnet, and to a lesser degree antithetic to the abundance of clinopyroxene. Approaching amphibole's upper pressure limit, the residual mineral assemblages would be termed amphibole eclogites. Synthesized amphiboles are calcic and classify with increasing pressure as tschermakite and pargasite for 800 °C [$(Na + K)_A$: 0.4–0.5, Si: 6.3–6.2], and as pargasite for 900 and 950 °C [$(Na + K)_A$: 0.5–0.6, Si: 6.1–6.0] (Hawthorne 1981).

Quartz appears on the solidus between 0.8 and 1.0 GPa, and its thermal stability increases with pressure to the expected conversion to coesite (identified only in the subsolidus in this study) (Tables 2, 3; Fig. 1). Run 71 at 1.4 GPa and 800 °C is anomalous in that it contains quartz, whereas runs at adjacent pressures and temperatures do not. Run 71 also has anomalously low melt fraction relative to 800 °C runs at adjacent pressures. Liu's lab books, archived at the USGS in Menlo Park, record that some of the MORB + H_2O inner capsules were run alongside a second inner capsule containing MORB + H_2O + CO_2. Results of those exploratory mixed H_2O–CO_2 experiments were not reported in Liu et al. (1996) and Liu (1997), but it is possible that capsule 72 (MORB + H_2O + CO_2 at 1.4 GPa and 800 °C) was mistaken for its companion capsule 71 (MORB + H_2O), accounting for the low melt fraction and anomalous high-temperature quartz stability.

Accessory minerals consist of apatite in all run products through 900 °C, rutile at greater than 1.2–1.4 GPa, versus ilmenite or titanite at lower pressures, clinozoisite (or zoisite) from 0.9 to 1.9 GPa at 700 °C and up to 750 °C at 1.2 GPa, as well as zircon and Fe-sulfide identified sporadically in run products from 700 to 750 °C (Tables 2, 3). Fe-sulfide also forms minute blebs (< 1 μm) in garnet and clinopyroxene in 2.6 and 2.8 GPa run products but was not found in contact with glass. Atypical accessory minerals are a grain of Al_2SiO_5 (presumably kyanite) identified for 700 °C and 3.0 GPa (run 182), and grains of phengite and staurolite for 700 °C and 2.6 GPa (run 128). Those runs were sub-solidus, and it is unknown if their atypical accessory minerals were metastable, although the run durations were long and similar to runs lacking those phases. Allanite, monazite, and xenotime were searched for but not found, consistent with the low concentrations of incompatible trace elements in the MORB starting material, and with the high abundances of amphibole and garnet that accept high concentrations of Y and heavy REE.

Pressure–temperature location and shape of the solidus

The onset of complete miscibility between aqueous fluid and hydrous melt was not investigated, but we follow Kessel

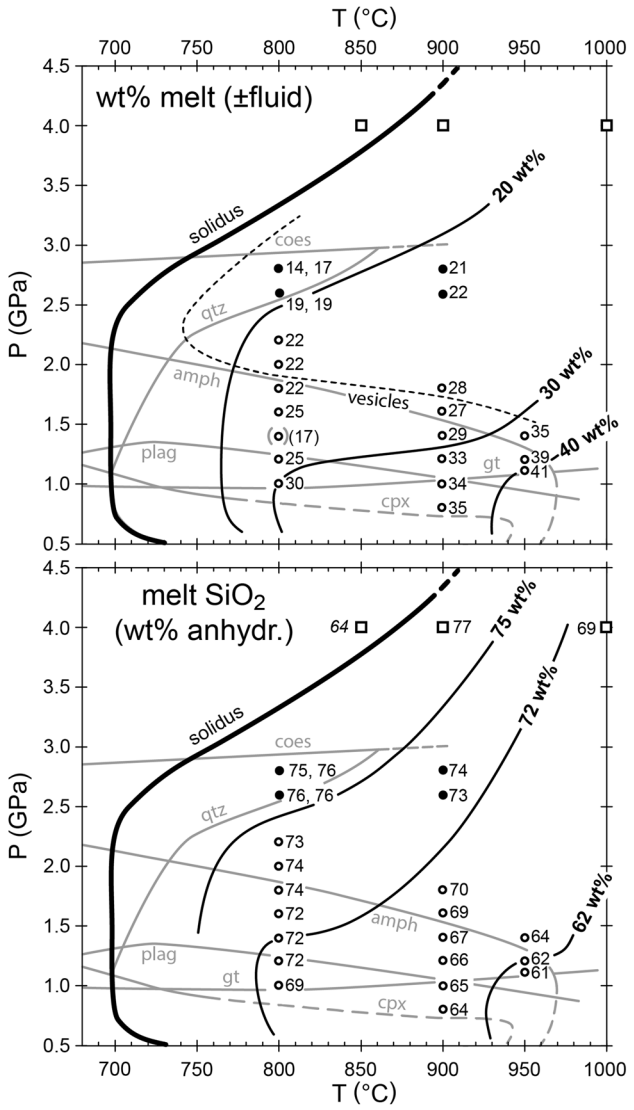

Fig. 3 Upper: Isopleths of wt% reconstructed melt (±fluid) synthesized in JDF MORB + 4 wt% H_2O determined by least squares multiple regression (Table 2). Lower: Isopleths of anhydrous-normalized SiO2 concentrations (wt%) of reconstructed melt (±fluid) synthesized from JDF MORB + 4 wt% H2O (ST-4). Open circles are experiments from Liu (1997), filled circles are new runs for this study, squares show anhydrous-normalized SiO_2 of fluid (italics, 850 °C) and melt (900, 1000 °C) synthesized in K-free haplobasalt at 4 GPa (Kessel et al. 2005b) Dashed black line shows limit of spherical bubbles > 10 μm, bracketed at 800 and 900 °C, and extrapolated at lower temperatures. Anomalous low weight-fraction melt (±fluid) at 1.4 GPa and 800 °C is considered suspect and may be due to misidentification of run mounts, as discussed in text

et al. (2005b) and Schmidt et al. (2004), who present evidence that the second critical endpoint for the hydrous basaltic eclogite solidus lies between 5 and 6 GPa. Therefore, we refer to melt, melting, and the H_2O-saturated solidus. The identification of glass in four 700 °C runs from 0.8 to 2.2 GPa lowers the known H_2O-saturated solidus of this MORB from that of Liu et al. (1996) and Liu (1997) to about 700 °C over that pressure interval, similar to the results of previous studies of H_2O-saturated basalt melting (Yoder and Tilley 1962; Hill and Boettcher 1970; Lambert and Wyllie 1972; Schmidt and Poli 1998; Klimm et al. 2008), and about 50 °C hotter than the H_2O + phengite-saturated basaltic eclogite solidus (Schmidt and Poli 1998; Schmidt et al. 2004). Glass in 700 °C run products has low back-scattered X-ray brightness relative to other phases, continuously fills interstices between mineral grains, contains scattered spherical voids (bubbles), and damages under a focused electron beam. Since glass was not found in all run products from 700 °C and 0.8–2.2 GPa, the solidus is probably close to 700 °C for the studied composition, and there were probably small inaccuracies in the temperatures of those runs causing inconsistent presence of glass. Open pores are widespread between mineral grains in run products from pressures greater than 2.2 GPa at 700 °C, but glass has not been identified, and above that pressure the solidus is drawn (Fig. 1) with a positive slope to join the 4.0 GPa H_2O-saturated solidus of K_2O-free basaltic eclogite bracketed between 850 and 900 °C by Kessel et al. (2005b).

Melting behavior and melt (± fluid) composition

Glasses are generally silicic, normalized on an anhydrous basis, spanning from high-silica rhyolite at the coolest temperature and greatest pressure down to silicic andesite at the hottest temperature and lowest pressure (ST-4). Glass compositions are more evolved at greater pressures for each investigated temperature. Sparse spherical bubbles, > 10 microns across, in lower pressure glasses may record the stability field of an aqueous fluid (Table 2), but the solubilities of H_2O in melt and of Na_2O and SiO_2 in aqueous fluid are insufficiently known to quantify fluid and melt abundances. Isopleths of the abundance of melt (± fluid) have positive *P*/*T* slopes, with the abundance of melt (± fluid) diminishing with increasing pressure (Fig. 3), consistent with a positive *P*/*T* slope for the H_2O-saturated solidus at > 2.2 GPa.

Melting behavior and melt compositions are divisible into three broad *P*–*T* regions. At pressures greater than the stability of amphibole, the fraction of melt (± fluid) rises from the (inferred) H_2O-saturated solidus to ~ 20 wt% over an interval of 80–120 °C. Quartz is lost at close to 20 wt% melting, and melt fraction then remains almost constant over a broad temperature span: melt fraction increases by only an additional 10 wt% for a further 150–200 °C of heating (Fig. 3). Anhydrous-normalized melt (± fluid) compositions remain rhyolitic (≥ 72 wt% SiO_2) to as much as 200 °C above the H_2O-saturated solidus (Fig. 3). This "plateau" pressure–temperature region of moderate melt fractions and uniformly silicic melt compositions corresponds with quartz-free

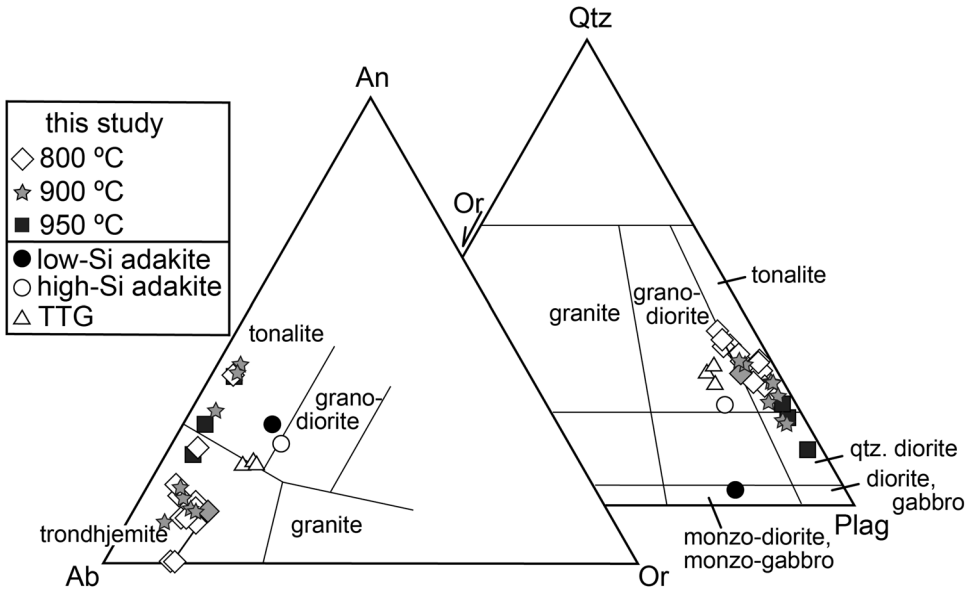

Fig. 4 Reconstructed melt (±fluid) (ST-4) plotted on the granitoid classification diagrams of Barker (1979) (left) and Streckeisen (1976) (right). Shown for comparison are average high-silica and low-silica adakites, and averages of Archean and younger tonalite–trondhjemite–granodiorite suites (Martin et al. 2005). Gray-shaded diamond is reconstructed melt (±fluid) for run 2238 using higher-Na clinopyroxene composition from run 2241. The Barker diagram shows molar albite (Ab), anorthite (An), and orthoclase (Or) converted from weight CIPW norms. Compositions are plotted in the Streckeisen (1976) diagram as CIPW normative albite + anorthite (Plag), quartz (Qtz), and orthoclase (Or)

eclogite residual mineral assemblages. The temperature range for hydrous rhyolitic melt coexisting with eclogite may narrow at pressures > 3 GPa (Fig. 3), but few results are available to assess this (Kessel et al. 2005b).

A low-pressure melting region (≤ 1.4 GPa) corresponds with residual mineral assemblages containing amphibole + minor plagioclase. In this region, melt (± fluid) abundance rises from the H_2O-saturated solidus to ~ 30 wt% over a 100 °C interval (Fig. 3). Increasing the abundance of melt (± fluid) by an additional 10 wt% requires 100–150 °C of further heating, only attaining ~ 40 wt% close to the maximum thermal stability of amphibole. Anhydrous melt compositions change gradually (Fig. 3), consisting of rhyolite to ~ 30 wt% melting, rhyodacite and dacite from 30 to 40 wt% melting, and silicic andesite near the upper temperature limit of amphibole (~ 950 °C).

An intermediate pressure region, consisting of amphibole + clinopyroxene + garnet residual assemblages, is also transitional in its melting behavior. Abundance of amphibole diminishes sharply with increasing pressure across this melting region. Because the reaction of amphibole to clinopyroxene + garnet + melt is continuous, melt fraction does not increase crossing the amphibole-out boundary (Fig. 3). Melts are rhyolitic to 100–150 °C hotter than the H_2O-saturated solidus, with SiO_2 concentrations gradually diminishing with increasing temperature to silicic andesite values near amphibole's maximum thermal stability (Fig. 3).

Melts can also be classified as trondhjemitic, tonalitic, and quartz dioritic (Fig. 4), in accord with prior studies of the near-solidus melting of low-K basalts (Helz 1976; Rapp et al. 1991; Rushmer 1991; Rapp and Watson 1995; Winther 1996; Wolf and Wyllie 1994; Skjerlie and Patiño Douce 2002). Higher-pressure melts plot in more evolved fields for each temperature investigated, consistent with greater proximity to the solidus and lesser extents of melting, as previously documented by Winther (1996) for eclogite-facies melting of hydrous low-K basalt. None of the melts have high Mg numbers (Mg#: Mg/Mg + ΣFe molar), but contrary to common experience, their Mg#s increase slightly with increasing SiO_2 (Fig. 5), which correlates with lower temperatures and greater pressures. This increase in melt Mg# with pressure probably results from the greater abundances of almandine-rich garnet that reduce Fe/Mg of the coexisting melt. Although the majority of synthesized melts would classify as tholeiitic due to high FeOt/MgO (Miyashiro 1974), the higher pressure 800 and 900 °C melts approach and straddle the tholeiitic—calc-alkaline boundary.

Trace element concentrations of glasses and apparent bulk solid–liquid partition coefficients

Trace element concentrations of glasses (ST-3) accord with residual mineral assemblages. Glasses coexisting with garnet have low concentrations of Y and heavy REE, and those

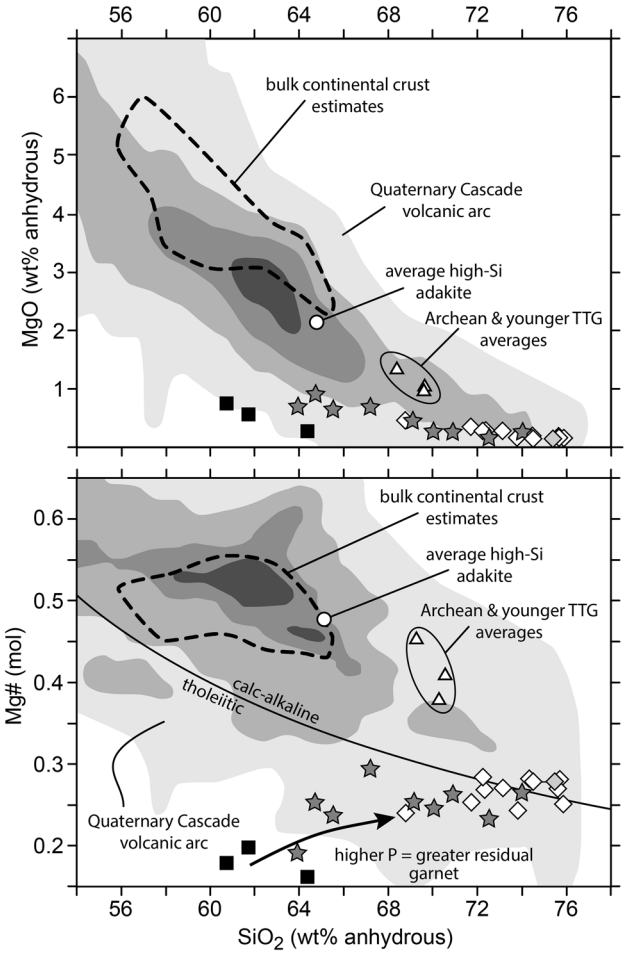

Fig. 5 MgO (wt%) and molar Mg# (Mg/[Mg + ΣFe]) versus anhydrous-normalized SiO_2 (wt%) of reconstructed melt (± fluid) synthesized in JDF MORB + 4 wt% H_2O (ST-4). Diamonds, stars, and squares are results from 800, 900, and 950 °C, respectively. Tholeiitic–calc-alkaline boundary is converted from the FeOt/MgO versus SiO_2 diagram of Miyashiro (1974). Shown for comparison are average high-silica adakite (circle), and averages of Archean and younger tonalite–trondhjemite–granodiorite suites (triangles, Martin et al. 2005). Gray-shaded diamond plots the reconstructed melt (± fluid) composition for run 2238 using higher Na clinopyroxene composition from run 2241. Higher-pressure melts are generally displaced to greater Mg# and normalized SiO_2 for each temperature. Shaded fields show volcanic rock compositions from the Quaternary Cascade magmatic arc, western USA and Canada, with darker shading signifying greater abundance of samples (see Supplemental References File for sources of Cascade analyses). Heavy dashed line encompasses estimates of the bulk composition of the continental crust (BCC) (Hacker et al. 2015)

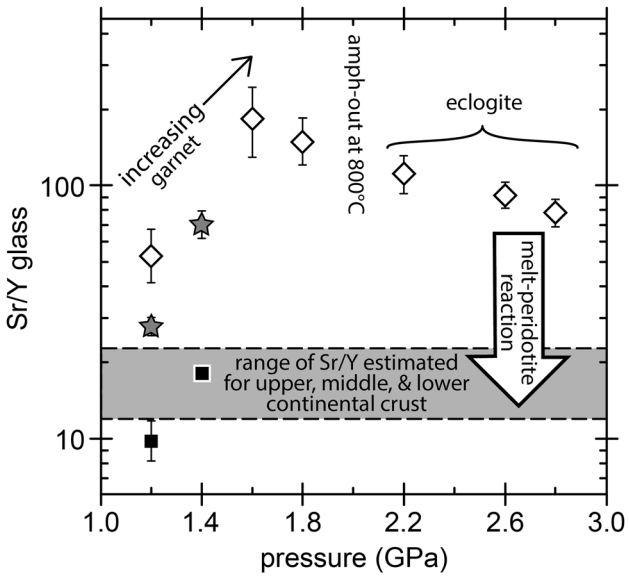

Fig. 6 Average Sr/Y of glass (ST-3) plotted versus synthesis pressure. Diamonds, stars, and squares are results from 800, 900, and 950 °C, respectively. Uncertainty brackets are one standard deviation of the mean. Open arrow shows general shift in Sr/Y of eclogite partial melt reacting with peridotite (this paper and Kelemen 1995; Kelemen et al. 2003a, b, c, 2014). Gray shaded bar shows range of estimates of the Sr/Y of the continental crust compiled and produced by Hacker et al. (2015)

coexisting with rutile or titanite also have low concentrations of Nb and Ti. Concentrations of the light REE, Ba, Sr, U, and Th are strongly enriched in glasses, an exception being titanite-bearing run 70, in which U and Th are less strongly enriched and the light REE are depleted relative to the bulk sample. Glass Sr/Y increases strongly with decreasing temperature (lower melt fraction), attaining values of 80–150 at 800 °C, but only 10–20 at 950 °C (Fig. 6). Less prominent is that glass Sr/Y also generally increases with pressure for each temperature, consistent with greater modal garnet, although the maximum Sr/Y at 800 °C is in the amphibole eclogite stability field close to amphibole's upper pressure stability limit.

Apparent bulk solid/liquid partition coefficients (*Ds*) can be estimated from the concentrations of trace elements in glass (ST-3), the bulk sample (Table 1), and melt (± fluid) fractions (Table 2), similar to the approach of Klimm et al. (2008). This approach represents a solution for *D* of the batch equilibrium exchange equation:

$$\frac{C_l}{C_o} = \frac{1}{D + F[1 - D]},$$

where *F* is melt fraction, and C_o and C_l are the bulk and melt trace element concentrations. Supplemental Table 5 (ST-5) presents weighted-average apparent batch partition coefficients for residual mineral assemblages consisting of rutile–quartz eclogite, rutile-amphibole eclogite, and ilmenite–garnet clinopyroxenite, as well as a single estimate for titanite-garnet hornblendite. Weighted standard errors propagate an assumed 5 relative-percent uncertainty in *F* and the standard deviation in average glass concentration; where

only one glass analysis was available, the average standard deviation from other runs was employed.

A shortcoming of this batch approximation is the implicit assumption that minerals are homogeneously equilibrated with liquid. Diffusion of REE in garnet is sensitive to temperature, pressure, fO_2, and possibly also REE concentration. The "high concentration" diffusion equation of Bloch et al. (2015) indicates that it would require ~ 1.6 Myr for REE to diffuse over a characteristic distance ($x = [D_t]^{1/2}$, where D_t is diffusion coefficient) of 10 microns in garnet at 800 °C and 2.8 GPa. "Low concentration" REE diffusion in garnet would be about 1.6 log units faster at these conditions (Tirone et al. 2005; Bloch et al. 2015), still requiring ~ 40 kyrs to equilibrate across 10 microns. Thus, garnets synthesized in this and in other experimental studies at similar conditions grew much faster than they could have equilibrated diffusively. Garnet in this study and in the eclogite melting studies of Klimm et al. (2008) and Kessel et al. (2005b) are known to have relatively Fe-rich interiors and Mg-rich rims. Diffusion of REE and Y in garnet is similar to or slower than the diffusion of divalent cations (Carlson 2012), therefore, the preservation of Fe–Mg zoning in garnet confirms that growth zoning of REE and Y has not been erased diffusively.

Failure of growth zoning to equilibrate with melt can influence apparent partition coefficient (D) values considerably, particularly for compatible elements, as can be seen by an alternate derivation for D treating the minerals as having grown fractionally under surface equilibrium but with no diffusive homogenization:

$$\frac{C_l}{C_o} = F^{D-1}.$$

Weighted-average apparent partition coefficients and propagated uncertainties for this fractional growth approximation are also presented in Supplemental Table 5. These "fractional-growth" partition coefficients differ in that the apparent Ds for incompatible elements are moderately increased, and those for the compatible elements are substantially diminished, relative to the "batch" partition coefficient solutions. True partition coefficient values are likely to lie between the "batch" and "fractional-growth" approximations. The eclogite melting partitioning results of Kessel et al. (2005a) derive from direct trace element analyses of liquid, clinopyroxene, and garnet, so they may be more accurate, but this depends on the degree to which the rims of zoned minerals were analyzed successfully and their interiors were avoided, which can be challenging due to the large size of routine LA-ICPMS analysis spots and the short distances for diffusive equilibration attained at the experimental conditions.

Our apparent batch partition coefficient patterns for rutile–quartz eclogite and rutile–amphibole eclogite (Fig. 7) are similar to literature results for rutile eclogite (Kessel et al. 2005a; Klimm et al. 2008), with high bulk Ds for the heavy REE, Y, Ti, and Nb, and low Ds for Ba, K, and Sr. Shared subtleties are that $D_{Th} > D_U$ and that $D_{Zr} \geq D_{Hf}$, for reasons discussed in Klimm et al. (2008). Differences are that Ds for rutile–quartz eclogite and rutile–amphibole eclogite in the present study, although similar to each other, are on the low side of the literature values, particularly for the light REE, Th, and U, which may be due to the simpler accessory mineral assemblage in the present study (apatite, rutile), versus prior studies, with "doped", elevated REE and other trace element

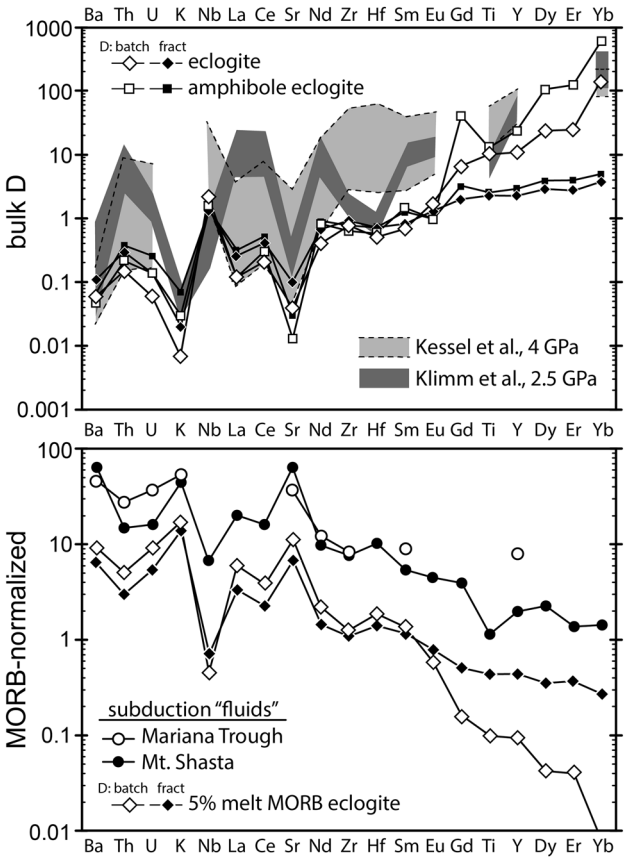

Fig. 7 Upper: Average solid/liquid partition coefficients (Ds) for eclogite (diamonds) and amphibole eclogite (squares) residual mineral assemblages (ST-5) compared with ranges of residual eclogite Ds from 4 GPa (Kessel et al. 2005a) and 2.5 GPa (Klimm et al. 2008). Open symbols—values assuming fully equilibrated experimental minerals, filled symbols—values assuming fractional growth zoning. Lower: MORB-normalized (Gale et al. 2013) trace element concentrations for subduction zone fluids (Stolper and Newman 1994; Grove et al. 2002), and 5 wt% eclogite-facies partial melt of MORB determined with D values derived assuming full equilibration of experimental minerals (open diamonds), and assuming fractional growth zoning (filled diamonds)

contents, which also produced allanite. The fractional-growth approximations for the present study differ chiefly in the much lower apparent *Ds* for the middle-to-heavy REE and Y.

There are close similarities between the trace element abundance patterns of subduction fluids inferred from the geochemistry of convergent margin volcanic rocks (Stolper and Newman 1994; Grove et al. 2002) and a modeled low degree partial melt of MORB using our eclogite facies *Ds* (Fig. 7). The chief difference is that the inferred subduction fluids have greater trace element concentrations by about a factor of 10, but this is partly due to those concentrations having been derived for an aqueous medium, free of silicate melt components. Another obvious distinction is the strong depletion in the heavy REE, Y, and Ti for eclogite partial melt calculated with "batch" *D* estimates that assume full equilibration of synthesized minerals. The partial melt calculated with "fractional-growth" *D* values, assuming growth zoning of synthesized minerals, has a trace element pattern that is more similar to inferred subduction fluids. This disparity highlights a continuing need for more accurate eclogite-melting *Ds*, particularly for the compatible elements.

Absence of allanite

Klimm et al. (2008) synthesized allanite in trace element-doped hydrous basalt at 2.5 GPa and 800–900 °C and developed an expression for the exchange of light REE between melt and an epidote-series mineral. That expression forms the basis of some proposed methods to estimate the temperature of subducting slabs as they release aqueous fluid or melt (Cooper et al. 2012; Plank et al. 2009). In our study, detailed SEM and electron microprobe examinations failed to reveal an epidote mineral in any run hotter than 750 °C. The absence of allanite in run products with natural MORB REE concentrations suggests that the exchange reaction expression of Klimm et al. (2008) is insufficient to predict epidote saturation. Skora and Blundy (2012) discuss how doping with some but not all essential chemical components can give misleading saturation results for accessory minerals. Clinozoisite (or zoisite) was synthesized at 750 °C and 1.2 GPa, and at 700 °C through 1.8 GPa (Table 3), so an epidote-series mineral may be residual to partial melting in localities where subducting MORB exceeds solidus temperatures at depths shallower than dynamic models predict for present-day subduction systems.

Applications

Density and fate of melting residues

Due to greater modal garnet, densities of the synthesized residual mineral assemblages increase markedly with pressure (Fig. 8). As expected, eclogite-facies residual assemblages are negatively buoyant relative to peridotite and would descend into the mantle. Residual assemblages formed at lower pressures may be density-stable relative to peridotite, or not, depending on temperature. Amphibole-dominated residual assemblages would be density-neutral at 800 °C and pressures through 1.4 GPa but are strongly negatively buoyant by 1.6 GPa (Fig. 8). Mineral residues become negatively buoyant relative to peridotite at slightly lower pressures of 1.0–1.4 GPa for residual assemblages with less amphibole produced by higher temperature melting. These considerations indicate that basaltic amphibolites can be density-stable in a narrow depth region beneath the base of the continents (1.0–1.4 GPa), even in the presence of H_2O and partial melting, unless temperatures exceed 900 °C (possibly > 950 °C for purely dehydration melting). Steady-state conductive geotherms yielding surface heat flows > 80 mW m^{-2} would be required to attain such temperatures immediately beneath continental crust of typical thickness and composition (Chapman 1986). Although such values exceed the mean continental surface heat flow of 65 mW m^{-2} and the likely temperature at the base of the crust in stable continental interiors (Pollack et al. 1993), they are well within the range of observed heat flow and likely temperatures at the base of the crust in volcanic arc and rifting environments (e.g., Blackwell et al. 1990; Kelemen et al. 2003b, Plate 1).

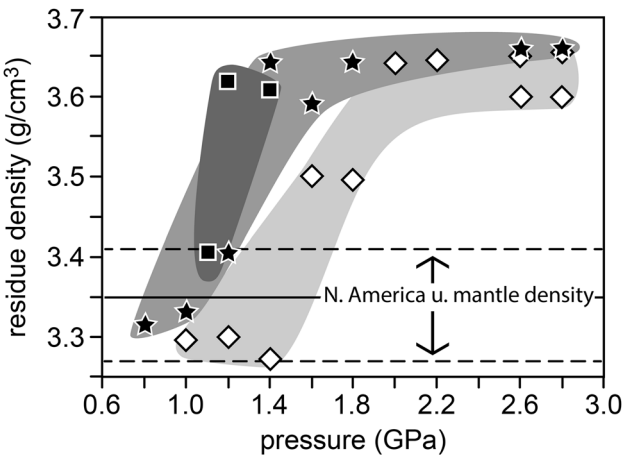

Fig. 8 Densities of residual mineral assemblages synthesized at 800 (diamonds), 900 (stars), and 950 °C (squares), calculated from mineral modes (Table 2) and molar mineral compositions assuming no excess volumes of mixing. Shading depicts the density ranges for the three run temperatures. The average density and density range of upper mantle peridotite beneath North America are from Mooney and Kaban (2010)

Phase-equilibrium limit on the melt-yield of hydrous eclogite-facies MORB

About half of the temperatures calculated for modern steady-state slab surfaces at sub-arc depths (Wada and Wang 2009; Syracuse et al. 2010) would exceed the H_2O-saturated solidus of phengite-bearing basaltic eclogite (Fig. 1), and exhumed subduction zone rocks can yield even higher metamorphic temperatures than are given by dynamic models (Hacker 2006; Penniston-Dorland et al. 2015), so low-degree melting of subducting basaltic eclogite is a viable process, so long as aqueous fluid is available, either trapped in subducting eclogites or introduced by metamorphic dehydration of other rock types within the subducting plate (serpentinite, chlorite peridotite). Little is known of the properties of such high-H_2O silicic liquids (ST-4), but extrapolation of composition–temperature relations (Giordano et al. 2008) indicates their viscosities could be as low as on the order of 10 Pa s at slab *P*/*T* beneath active arcs, facilitating their segregation even at low extents of melting. Hotter mantle early in Earth's history may also have fostered thicker oceanic crust, shallower subduction, and more widespread slab melting (Sleep and Windley 1982; Martin 1986). The "plateau" region identified for hydrous eclogite melting is of interest in that its onset marks diminished melt production with increasing temperature, indicative of a phase-equilibrium limit on melt productivity. Simulations of the hydrous melting of rutile–quartz eclogite at 2.8 GPa using the rhyolite-MELTS thermodynamic model (Gualda et al. 2012; Ghiorso and Gualda 2015) reproduce the onset of diminished melt production at ~ 825 °C and ~ 20 wt% melting for MORB + 4 wt% H_2O, corresponding to loss of quartz in the residual mineral assemblage (Fig. 9). At temperatures hotter than quartz-out, melt fraction is simulated as increasing by only 3–4 wt% per 100 °C of heating, consistent with the small increase of melt fraction determined experimentally from 800 to 900 °C. Simulations with greater and lesser total H_2O illustrate that the onset temperature for diminished melt production is strongly sensitive to total H_2O concentration, but also that the onset would correspond to exhaustion of residual quartz. The exhaustion of residual quartz is simulated as taking place at more than 15 but less than 25 wt% melting at 2.8 GPa over a wide range of H_2O concentrations. Thus, the ability of hydrous MORBs to produce melt in the eclogite facies is ≤ ~ 20 wt% at temperatures predicted for the top of subducting plates, and this limit is tied to the loss of modal quartz, consistent with the pressure–temperature coincidence of the quartz-out boundary and the 20 wt% melting isopleth (Fig. 3).

Limited melt productivity of hydrous quartz eclogite results from a multiple saturation point between liquid, quartz, clinopyroxene, and garnet that sits in a deep thermal well across a range of H_2O concentrations. At the lowest melt fraction investigated, corresponding to the lowest temperature and greatest pressure, the reconstructed melt (± fluid) composition is weakly peralkaline, and the melting reaction is peritectic: quartz + clinopyroxene = liquid + garnet (Fig. 10)[2]. At slightly greater extents of melting, liquids project within the quartz−clinopyroxene−garnet volume, and quartz + clinopyroxene + garnet saturated melting is pseudo-eutectic. For both peritectic and pseudo-eutectic melting, the depth of the thermal well restricts the degrees of melting attainable at the top of subducting basaltic plates. The silicic composition of the near-solidus melts ties their yield to the modal quartz of the source eclogite. Eclogite-facies melting experiments on drier low-K basalts (H_2O: ~ 0.7 to ~ 1.7 wt% based on LOI) find the 20 wt% melting isopleth in the vicinity of 1000 °C at 0.8–3.2 GPa, 200–300 °C hotter than the H_2O-saturated basaltic eclogite solidus (Rapp 1995; Rapp and Watson 1995). Likewise, the empirical fit of Winther (1996) to melting experiments on hydrous low-K basalt predicts an increase of melt fraction at 2.8 GPa of only 0.2 wt% between 800 and 900 °C for 1 wt% total H_2O, or

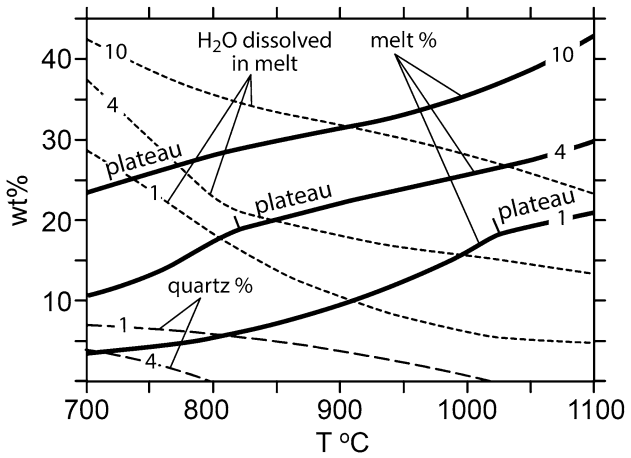

Fig. 9 Results of rhyolite-MELTS simulations of 2.8 GPa batch melting of JDF MORB plus 1, 4, and 10 wt% H_2O showing weight percent of melt (solid lines), quartz (long dashed lines), and H_2O concentration in melt (short dashed lines), versus temperature. Lines are labeled with the bulk H_2O concentration (wt%) of the simulation, and "*plateau*" marks the region of suppressed melt production following quartz-exhaustion. Simulations involve rhyolite-MELTS version 1.2.0. Rhyolite-MELTS does not identify a H_2O-saturated solidus at 2.8 GPa as cool as 650 °C, likely due to shortcomings in treating H_2O solubility in melt and non-accounting for alkalis and silica partitioned into aqueous fluid

[2] Another potential peritectic reaction is: $3CaMgSi_2O_6$ clinopyroxene + $4NaAlSi_2O_6$ clinopyroxene = $2Na_2O$ melt + $8SiO_2$ melt, quartz + $1Ca_3Al_2Si_3O_{12}$ garnet + $1Mg_3Al_2Si_3O_{12}$ garnet but is inconsistent with the melt – mineral topology in Fig. 10.

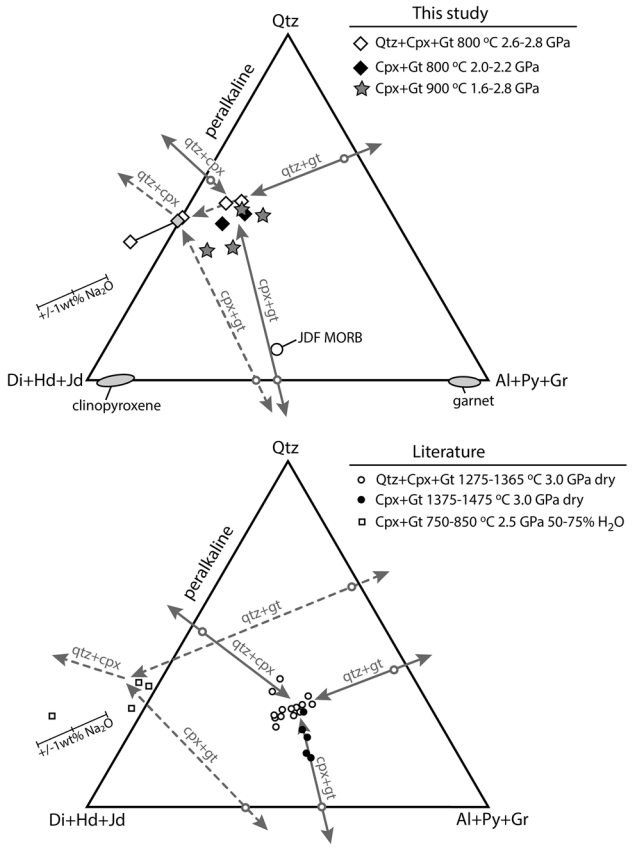

Fig. 10 Eclogite-facies reconstructed melt compositions normalized anhydrous and projected into the system quartz (Qtz), Diopside–Hedenbergite + Jadeite (Di + Hd + Jd), and almandine–Pyrope + Grossular (Al + Py + Gr). Projection is through rutile, apatite, and orthoclase components. Gray lines show schematic cotectics labeled with saturating minerals, thermal divides (circles), and down-temperature directions (arrows). Solid lines depict lower-H_2O configurations with quartz–clinopyroxene–garnet pseudoeutectic, and dashed lines depict higher-H_2O peritectic melting. Upper plot shows results from this study (ST-4); lower plot shows the literature results at higher (Klimm et al. 2008) and lower H_2O concentrations (Pertermann and Hirschmann 2003). Gray diamond plots reconstructed melt (± fluid) for run 2338 derived with higher-Na clinopyroxene from run 2241. Shaded fields show projected compositions of synthesized eclogite-facies clinopyroxene and garnet (ST-2). Glasses from Klimm et al. (2008) were reconstructed as for this study incorporating a fictive Na_2O phase to address Na-loss during electron-probe analyses. Projection components in equal-oxygen units, cations in mol fraction: Quartz = [2(Si–Ca)−6K−4Na−2(Fe + Mg) + 3.333P]/sum. Almandine-Pyrope = [3Al −2Ca−3(K + Na) + 2(Fe + Mg) + 3.333P]/sum. Grossular = [3Al + 2Ca−3(K + Na)−2(Fe + Mg)−3.333P]/sum. Orthoclase = 8K/sum. Jadeite = 6Na/sum. Diopside-Hedenbergite = [−4.5Al + 3Ca + 4.5(K + Na) + 3(Fe + Mg)−5P]/sum. Rutile = 2Ti/sum. Apatite = 4.167P/sum. sum = Σcomponent numerators

2.3 wt% for 4 wt% total H_2O. Thus, the walls of the thermal well are very steep. Initially peritectic melting, passing to eutectic-like, in a deep thermal well can be expected as a general property of basaltic quartz eclogites undergoing hydrous anatexis in subducting slabs, restricting their melting to low extents and to rhyolitic compositions.

The highly silicic melt compositions and the strong reduction of melt productivity at quartz exhaustion lead to a simple relation between fluid-fluxed melt productivity and the modal quartz of the source basaltic eclogite. For estimated present-day, steady-state subducting slab conditions, melt productivity from hydrous basaltic eclogites is restricted to no more than about twice the weight fraction of quartz originally present in the source. This general limit can be inferred by two approaches: (1) anhydrous compositions of the quartz-saturated eclogite partial melts (ST-4) are approximately 0.51–0.56 quartz:0.46–0.43 jadeite:0.03–0.01 diopside + hypersthene (wt units converted from CIPW norms). Dissolved H_2O will reduce these values slightly, but they indicate that the melts are about 50 wt. percent normative quartz. (2) Stoichiometry of the integrated melting reaction can be approximated by estimating subsolidus modes and then differencing against synthesized phase proportions (Table 2). Amphibole-free eclogite-facies subsolidus modes of JDF MORB + 4 wt% H_2O were estimated for 2.6 and 2.8 GPa by least-squares mass balance using 800 °C mineral compositions, first assigning all K_2O to phengite and all P_2O_5 to apatite. The average melting reaction for 2.6 and 2.8 GPa integrated to shortly beyond quartz exhaustion (900 °C) is (wt units):

$$1\ \text{liq} = 0.13\ \text{gt} + 0.12\ \text{cpx} + 0.48\ \text{qtz} + 0.07\ \text{pheng} + 0.01\ \text{rut} + 0.18\ \text{vapor} + 0.01\ \text{ap}.$$

Again, production of one mass unit of melt consumes about half that mass of quartz, so at quartz-exhaustion, the mass fraction of melt is close to twice the source's quartz mass fraction at the solidus. Degrees of melting appreciably greater than twice the source's original quartz mass fraction would require temperatures substantially hotter than the quartz-out limit, which are probably unattainable in modern, tectonically ordinary subducting plates at subarc depths.

A solidus mode for the average whole-rock composition of 5487 basalts, gabbros, diabases, and dolerites from submarine spreading ridges (http://www.earthchem.org/petdb, download of 21 January 2017; Lehnert et al. 2000), including rocks classified as altered, obtained by converting into 800 °C 2.8 GPa garnet, clinopyroxene, rutile, quartz, and apatite, plus phengite, yields 9 wt% quartz and 2.6 wt% phengite. Thus, the exhaustion of quartz would occur at about 20 wt% melting in average subducting mafic igneous rocks. Melting up to the quartz-out limit will be controlled by temperature and the availability of H_2O, but all such liquids will be highly silicic, ruling out production of primitive andesites (e.g., adakites) solely by partial melting of basaltic eclogite undergoing ordinary subduction.

Direct production of andesite–dacite melts similar to the mean continental crust composition

Liquids with dacitic to silicic andesitic compositions (SiO_2: 65–60 wt%), similar to widespread granodioritic and tonalitic rocks of the continents, were only produced at the lower pressures and higher temperatures of the present investigation, close to the upper temperature limit of amphibole (Fig. 3). These andesitic–dacitic melts, however, have Mg#s and Mg concentrations too low to match common tonalities and granodiorites of the continental crust (Fig. 5). Kelemen (1995) and Martin et al. (2005) point out that this disparity is widespread among prior studies of the experimental melting of hydrous basalts at deep crustal through upper mantle pressures. Higher fO_2s raise the Mg#s of near-solidus partial melts of basalt by stabilizing magnetite (Sisson et al. 2005). Had the Liu (1997) experiments been performed with a more oxidizing buffer than quartz–fayalite–magnetite, the liquid Mg#s would be closer to those of common tonalities, granodiorites, and bulk continental crust. However, magnetite stabilization raises Mg# in melts by lowering their total Fe concentrations, not by increasing their Mg concentrations, whereas experimental basaltic partial melts are deficient in Mg, relative to common tonalities, granodiorites, and estimated bulk continental crust (Fig. 5).

An important general conclusion is that direct melts from hydrous basaltic sources in the eclogite and amphibole eclogite facies are likely to be more silicic (rhyolites) than the common rocks of the continents, and that even the lower-silica amphibolite facies melts from base-of-continent depths are likely to have lower Mg and Mg# than the common igneous rocks of the continents, irrespective of the Mg content or oxidation state of potential basaltic sources (Fig. 5). Additional processes, such mixing of peridotite-derived basalts with silicic deep-crustal partial melts and with silicic residual liquids (Blatter et al. 2013) and reaction of silicic partial melts of subducting plates with hot peridotite of the mantle wedge (Kay 1978; Yogodzinski et al. 1995; Kelemen 1990, 1995; Kelemen et al. 2003c; Martin et al. 2005) probably act to yield the common igneous rocks of the continents or of their mafic parental magmas.

Reaction of eclogite partial melt with mantle wedge peridotite—trace elements

If they are to influence arc magmatism, low-degree partial melts of subducting slabs must transit and escape the hot mantle wedge. During transport through the mantle, reactions with peridotite can change the melts' major and trace element characteristics. Figure 11 presents two scenarios of basaltic eclogite partial melt reacting with mantle wedge peridotite illustrative of possible subduction early in Earth history. In both simulations primordial oceanic crust, itself formed by 10% MORB-like partial melting (Workman and Hart 2005) of undifferentiated bulk silicate earth peridotite (McDonough and Sun 1995), subducts and undergoes 5% hydrous eclogite-facies partial melting (*Ds* for slab partial melting are midpoint values between the fractional and batch estimates for eclogite in ST-5). Reactions of this eclogite partial melt with mantle wedge peridotite are modeled as (1) assimilation–fractional crystallization (AFC, DePaolo 1981), and (2) open-system critical melting (or reactive porous flow; Shaw 2000, and references therein). In both scenarios, the solid reactant is depleted MORB mantle (DMM) with *Ds* appropriate for spinel peridotite melting (Workman and Hart 2005). The AFC simulations set mass assimilated/mass crystallized to 1.1 to simulate increasing melt mass as melts ascend through hotter and shallower portions of the mantle wedge, whereas the open-system melting assumes a critical melt fraction of 0.015 and that the influx of a mass unit of slab melt leads to an equal mass unit of modal melting of the infiltrated peridotite ("β" = 1). Many additional refinements and permutations are possible but are beyond the scope of this study.

Trace element characteristics of peridotite-reacted eclogite partial melts, similar to common subduction magmas, are enrichment in alkalis, alkaline earths, light REE, and actinides, depletion in Nb (and Ta, although not analyzed or modeled in this study), and minor depletions of Zr and Hf. The nature of interaction differs in the two scenarios. For AFC, reaction-progress lowers the integrated ratio of eclogite partial melt to depleted mantle. Increasing melt mass thereby lowers concentrations of the more incompatible trace elements and raises concentrations of heavy REE, Y, and Ti in the product melt. As reaction progresses, the melt becomes more similar to a simple melt of the ambient peridotite. For open-system melting, reaction-progress involves transit of greater proportions of eclogite partial melt through the same mass of depleted peridotite. In the initial stages, the reacted melt is influenced strongly by contributions from the original peridotite, but as more eclogite partial melt transits the same mantle mass, the pooled melt becomes progressively more similar to the original infiltrating liquid (Fig. 11). In both cases, the exceptionally low concentrations of heavy REE, Y, and Ti of the infiltrating eclogite-derived melt are generally raised to values closer to equilibrium with the initial peridotite reactant (Kelemen et al. 2003c).

Notably, the positive Sr anomaly, $Sr/Sr^* = \left[\frac{Sr_N}{\sqrt[2]{Pr_N \times Nd_N}} > 1 \text{ or } \frac{Sr_N}{\sqrt[3]{Ce_N \times Nd_N^2}} > 1\right]$ of eclogite partial melts is preserved in the products of peridotite-melt reaction (Fig. 11). The eclogite-facies *D* for Sr is also low relative to those for Ce and Nd in the lower temperature results of Kessel et al. (2005a) and those of Klimm et al. (2008) (Fig. 7),

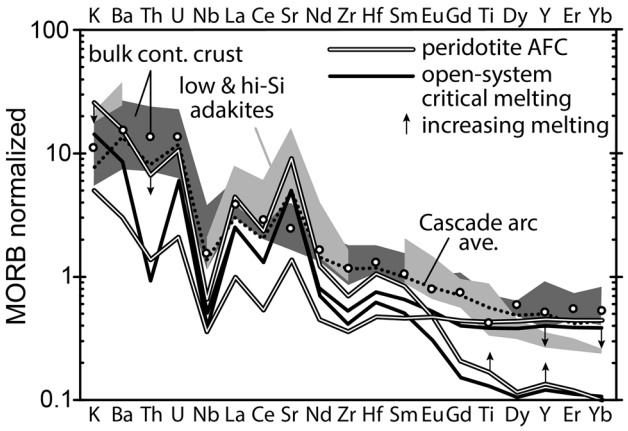

Fig. 11 MORB-normalized (Gale et al. 2013) trace element features of 5% partial melt of eclogite-facies primordial oceanic crust reacted with depleted MORB mantle by assimilation–fractional crystallization (white lines, AFC) and by open system critical melting (black lines). *Arrows* show direction of reaction progress. Dark gray field shows a range of estimates of the composition of the bulk continental crust (Hacker et al. 2015), with a commonly cited example (circles, Rudnick and Gao 2003). Light gray field encompasses average high- and low-Si adakites (Martin et al. 2005). Plotted AFC results are 1.1- and sixfold increases in melt mass for mass assimilated/mass crystallized = 1.1. Plotted open-system results are compositions of pooled melts for melt fractions of the infiltrated peridotite of 0.1 and 0.5 during mass infiltrating/mass melting = 1 and a retained melt fraction of 0.015. AFC and open-system calculations assume interaction with depleted MORB mantle and *Ds* appropriate for the spinel peridotite facies (Workman and Hart 2005). Primordial oceanic crust was calculated as a 10% melt of primitive mantle (McDonough and Sun 1995) also with spinel peridotite *Ds*. 5% partial melt of subducted primordial oceanic crust is calculated with the median eclogite-facies *Ds* from ST-5

therefore, positive Sr anomalies are robust features of low-degree eclogite partial melts and of eclogite-derived supercritical slab fluids. Such positive Sr anomalies are typical of many primitive arc basalts (Perfit et al. 1980; Bacon et al. 1997; Kelemen et al. 2003a, 2014), and of adakitic andesites and dacites thought to be derived via reaction of eclogite melts with mantle peridotite (e.g., Kay 1978). Average primitive (Mg# > 0.6) basalts from oceanic arcs have Sr/Sr* from 1.8 to 4.2; average primitive andesites range from 2.2 to 4.2 (Kelemen et al. 2003a, 2014).

In contrast, Sr/Sr* is significantly lower (range 0.5–1.4, median 0.8) in estimated compositions of bulk continental crust (Rudnick and Gao 2003; Hacker et al. 2015) and is similar to continental crust in many tonalite–trondhjemite–granodiorite suites (Martin et al. 2005). Several processes could reduce the size of Sr anomalies in continental crust relative to potentially parental arc magmas. Chief among these are (1) crystallization-differentiation or partial melting producing feldspar-rich cumulates or restites with high Sr/Sr* that are removed from the crust, and (2) chemical weathering that dissolves Sr in preference to the REE.

Loss of Sr to feldspar by igneous processes is supported by the general diminution of Sr anomalies passing from primitive (Mg# > 0.6) to more evolved (lower Mg#, higher SiO_2 and K_2O, lower MgO, CaO, and Al_2O_3) arc igneous rocks, notable exceptions being geographically localized, evolved high-Sr adakitic andesites and dacites. Production of bulk continental crust with a Sr anomaly in the vicinity of 1 by processes similar to modern subduction magmatism requires foundering into the mantle of dense cumulates and melting residues (Kelemen et al. 2003a, c; Jagoutz and Schmidt 2013; Tang et al. 2015) and/or relamination of buoyant, evolved lithologies during subduction-erosion, subduction of arc-derived sediments, and arc–arc collisions (Hacker et al. 2011, 2015; Behn et al. 2011; Kelemen and Behn 2016).

Apparent degrees of differentiation (or fractions of residual liquid) necessary to reduce Sr/Sr* to 1 ± 0.2, similar to estimated bulk continental crust, from a primitive parent are shown in Fig. 12 for the examples of the Quaternary Cascade and the oceanic western Aleutian (from Makushin Island and westward) magmatic arcs. Due to potassium's incompatibility during all but highly advanced solidification of arc magmas, fractions of residual liquid can be approximated by the K_2O concentration of a representative primitive magma divided by the K_2O concentration of a volcanic rock under consideration. Representative primitive-magma K_2O concentrations are estimated by the average and one standard deviation of published analyses of Quaternary arc volcanic rocks with Mg# ≥ 0.65 and MgO ≥ 6 wt%, giving similar values for the Cascade and Aleutian arcs of 0.8 ± 0.4 wt% (see Supplemental References File for data sources and also Behn et al. 2011 for a similar estimate).

Using the best-fit primitive magma K_2O concentration of 0.8 wt%, Quaternary volcanic rocks from the Cascade and Aleutian arcs that lack appreciable positive or negative Sr anomalies (1.0 ± 0.2) can be interpreted as residual liquid fractions most commonly of about 0.4 and of 0.35–0.7, respectively (shaded fields in Fig. 12), or products of about 60 and 65–30 wt% crystallization. Incorporation of crustal partial melts would not change these estimated melt fractions so long as potassium-rich minerals were not appreciably residual to melting, the crustal sources undergoing melting were similar in composition to the average parental arc magmas (or were derived from sources similar in composition to such parents), and melt was not retained appreciably in the source. This admittedly simple approach indicates that to yield mean continental crust with Sr/Sr* close to 1 by processes like present-day convergent margin igneous differentiation requires crustal-level production and loss to the mantle of originally plagioclase-rich (hence, high Sr/Sr*) cumulates and melting residues in a mass broadly similar to that of the preserved continents. These estimates are consistent with other geochemical and geologic studies that point

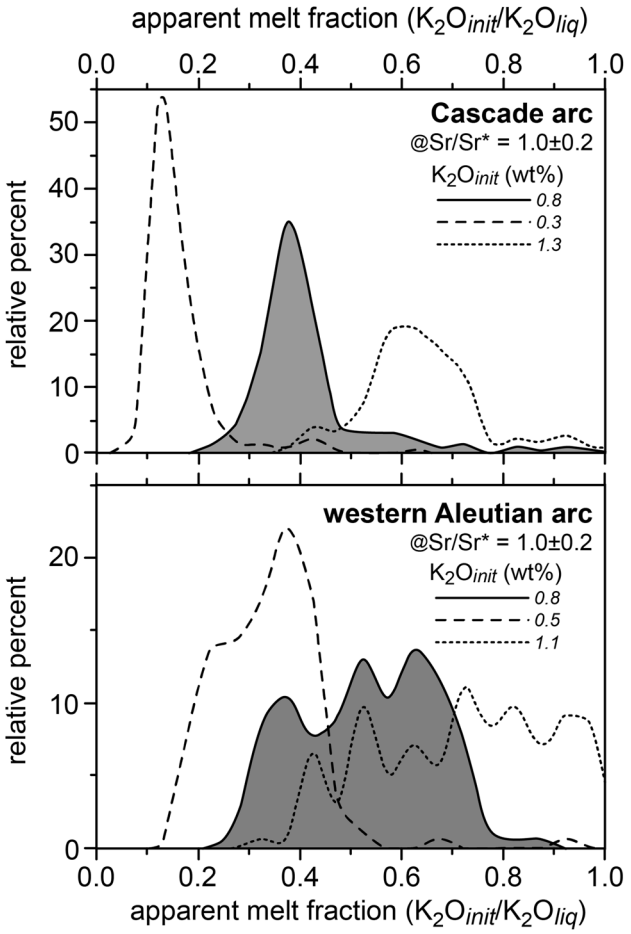

Fig. 12 Apparent residual melt fraction for volcanic rocks with Sr anomalies of 1.0 ± 0.2 from the Cascade (upper) and the oceanic western Aleutian (from Makushin west) (lower) magmatic arcs. Apparent melt fraction is $K_2O_{primitive}/K_2O_{sample}$ referenced to a representative primitive magma K_2O concentration (0.8 wt%) derived by averaging volcanic rock analyses with Mg# ≥ 0.65 and MgO ≥ 6 wt% from the respective arcs (solid lines with shaded fields). Results for ± 1 standard deviation in primitive magma K_2O concentration (± 0.5 wt%) are shown as dotted and dashed curves. Cascade results exclude rear-arc centers of Medicine Lake, Newberry, and the Simcoe Mountains. See Supplemental References File for sources of Cascade and Aleutian analyses

to the loss of cumulates and melting residues greater than or equal to the present continental mass (Kelemen et al. 2003a; Plank 2005; Jagoutz and Schmidt 2013; Tang et al. 2015; Kelemen and Behn 2016).

Recycling of subducted terrigenous sediments via relamination (Hacker et al. 2011, 2015; Behn et al. 2011; Kelemen and Behn 2016), can diminish the positive Sr anomalies of parental magmas and of the continents, respectively, due to such sediments' low Sr concentrations (Plank and Langmuir 1998). Terrigenous sediments are, however, chiefly derived by erosion of upper crustal rocks that have negative Sr anomalies (Taylor and McLennan 1985; Rudnick and Gao 2003; Hacker at al. 2015) generally attributed to feldspar fractionation at some prior stage, so removal of feldspathic cumulates or melting residues would still be required to yield net continental crust lacking a positive Sr anomaly via subduction magmatism. Alternatively, chemical weathering could preferentially remove Sr relative to the rare earth elements, thereby reducing the Sr anomalies of sediments and the continents.

Partial melting of mafic sources sufficiently shallow for appreciable residual plagioclase, such as near the base of the crust during collisional events or during flat-slab subduction, is an alternative explanation for subdued Sr anomalies in batholiths and the continents (Martin et al. 2005). Such conditions may be too shallow to stabilize rutile in mafic bulk compositions, but residual ilmenite (Table 2) might account for depletion of melts in high-field-strength elements. Return to the mantle of a large mass proportions of plagioclase-bearing melting residues would still be required to yield the intermediate composition of estimated bulk continental crust.

Reaction of slab partial melt with mantle wedge peridotite—major elements

Reactions between low-degree eclogite partial melt and peridotite were also investigated through pMELTS (Ghiorso et al. 2002) simulations of major elements, beginning with the average of 2.8 GPa, 800 °C melt (± fluid) compositions (ST-4) combined with depleted MORB mantle (DMM) (Workman and Hart 2005) in various fixed proportions. Reaction simulations commenced at 2.6 GPa by combining the 2.8 GPa eclogite melt with DMM in a fixed weight ratio of infiltrating melt to rock selected for the particular simulation, and the melt thereby produced was taken − 0.2 GPa shallower and combined again with DMM in the same weight ratio of infiltrating melt to rock. Calculations were thus stepwise repeated at increments of − 0.2 GPa, ceasing at a pressure appropriate for the top of the mantle (1.0 GPa). Temperature for each pressure step was fixed to that of the postulated wedge geotherm, which is equivalent to assuming that the mass of melt is small relative to its surroundings and moves sufficiently slowly that temperature is controlled by the ambient environment. Temperature first increases upward to a maximum at 2.2 GPa, then declines to the top of the mantle wedge. The simulations omit a region close to the slab where amphibole, chlorite, and serpentine may be stable, which is equivalent to treating such a zone as fully reacted, so slab melts pass through it unmodified. A further simplification was to fix fO_2 to that of quartz−fayalite−magnetite buffer, due to scant information on the oxidation state and oxidizing potential of slab partial melts. Supplemental Table 6 (ST-6) gives melt compositions, modes, and aggregate melt and rock masses relative to the initial melt mass

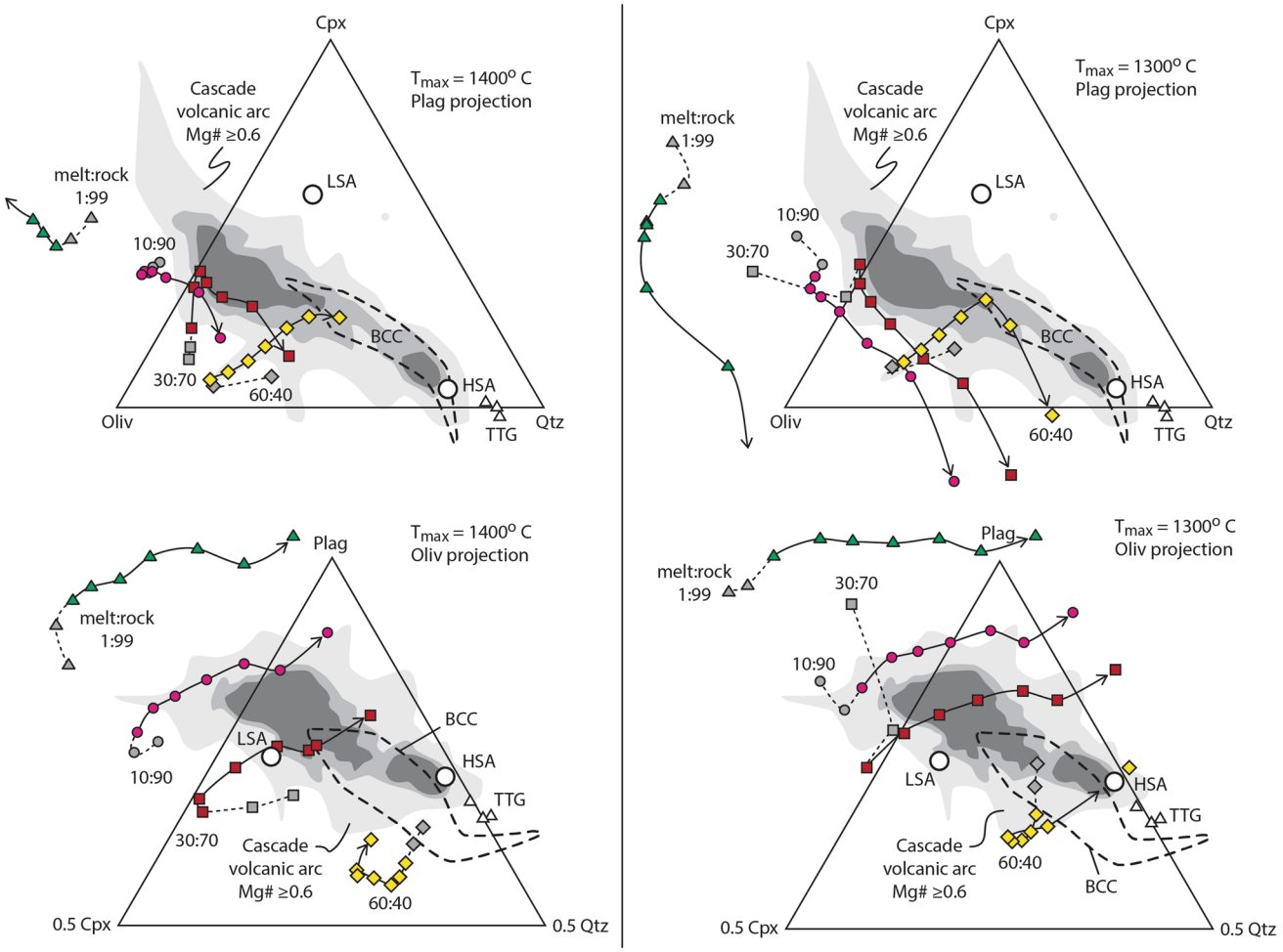

Fig. 13 Liquid compositions derived by stepwise reaction of average 2.8 GPa, 800 °C basaltic eclogite partial melt (+/− fluid) (ST-4) ascending through hot (left) and cool (right) mantle wedge peridotite over the pressure range 2.6–1.0 GPa (− 0.2 GPa per step). Liquid compositions are derived by pMELTS simulations (ST-6) distinguished by specified fixed ratios of infiltrating melt to peridotite per reaction step. Arrows point to lower pressure results, and gray symbols are deeper than the wedge thermal maximum (> 2.2 GPa). Compositions are converted to mineral components following Grove (1993). Shaded fields encompass Quaternary volcanic rocks of the Cascade magmatic arc with Mg# ≥0.6 (Supplemental References File gives sources for Cascade analyses); darker shading depicts more abundant compositions. White circles are average low- and high-silica adakites (LSA, HSA), triangles are average Archean and younger tonalite–trondhjemite–granodiorite suites from Martin et al. (2005), and heavy dashed line encompasses estimates of the bulk composition of the continental crust (BCC) (Hacker et al. 2015)

for scenarios with maximum wedge temperatures of 1300 and 1400 °C. Figure 13 shows the projected compositions of melts compared with Quaternary volcanic rocks of the Cascade magmatic arc with Mg# ≥0.6, Fig. 14 graphs the increase in melt mass relative to the initial melt mass passing up through the mantle wedge, and Fig. 15 shows the effect of olivine fractionation of 1.4 GPa melts as examples of liquids that segregate from the upper portion of the mantle wedge.

The principal result is that simulations with infiltrating melt to rock weight ratios from 30:70 to 60:40 per pressure step provide the closest match to natural arc basalts through andesites, with the higher melt:rock values yielding liquids with the greatest normative quartz, more similar to high Mg# andesites and dacites. Calculated melts have higher normative olivine than do most arc volcanic rocks, but this may signify that the parents to nearly all erupted arc basalts through andesites have crystallized some olivine (Fig. 15). Low infiltrating melt–rock ratios (< 10:90) yield consistently alkalic liquids, unlike common arc basalts, whereas the shallowest and lowest temperature liquids (< 1200 °C) can become corundum normative (negative Cpx component, Fig. 14), also unlike common arc magmas. Note, pMELTS overestimates the stability of clinopyroxene close to the peridotite solidus (Ghiorso et al. 2002), potentially exaggerating the predicted development of alkalic and peraluminous liquids. More sophisticated modeling would tie infiltrating melt:rock ratios to their transport properties, and would tie

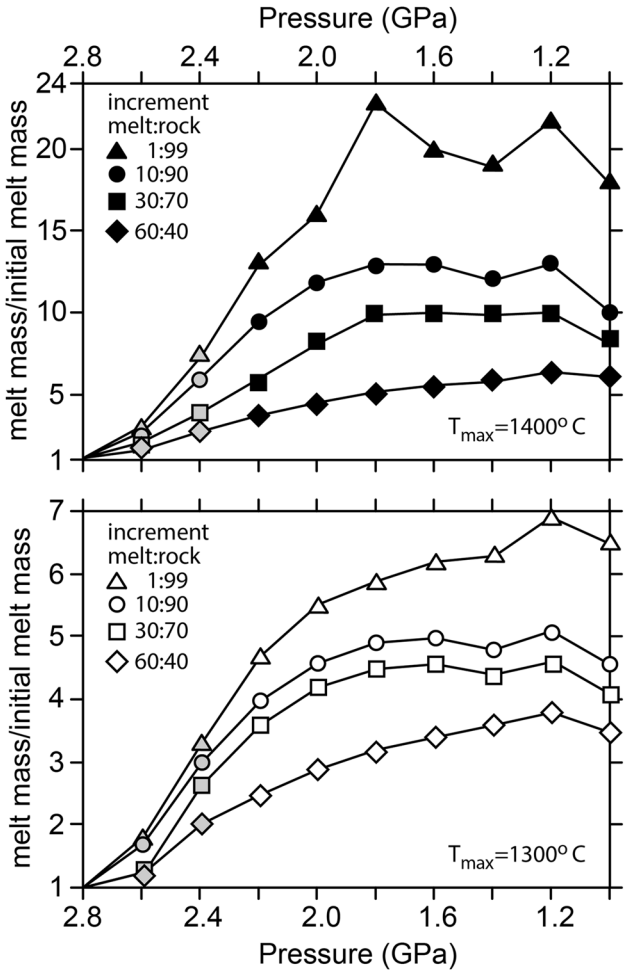

Fig. 14 Melt mass/initial melt mass versus pressure for the stepwise eclogite partial melt–peridotite reaction simulations of ST-6 and Fig. 13. Shaded symbols are deeper than the thermal maximum of the mantle wedge

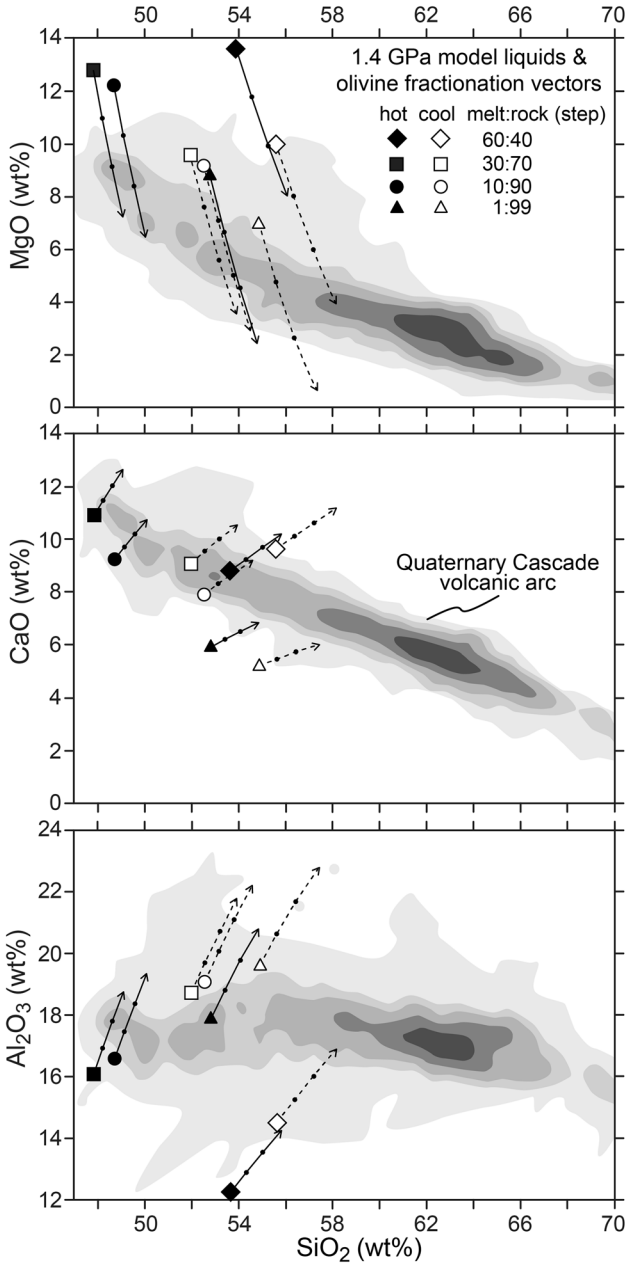

Fig. 15 Major oxide variation diagrams showing reaction-melts that might segregate from the upper portion of the mantle wedge (1.4 GPa, ST-6) and subsequently fractionate olivine (vectors), compared with Quaternary volcanic rocks of the Cascade magmatic arc (shaded fields, darker shading depicts more abundant analyzed compositions). Vectors show up to 15 wt% olivine fractionation with 5 wt% intermediate points (dots) and were calculated using the olivine forward-fractionation tool of Primelt3 (Herzberg and Asimow 2015). Supplemental References File gives sources for Cascade rock compositions

temperature to local melt flux and reaction enthalpies, but are beyond the scope of this study.

The roughly subequal ratios of infiltrating melt–rock (30:70–60:40), per reaction step, that yield the closest matches to parents for arc basalts and andesites, and for the bulk continental crust, may signify that most magmas that successfully transit the mantle wedge do so by channelized flow. Ascending melt is not a dispersed trace constituent, at least for magmas that escape the mantle wedge in abundance. Otherwise, transitional or alkalic arc magmas would be common. The simulations also suggest that parental arc melts are extracted from portions of the mantle wedge with temperatures ≥ 1200 °C. Otherwise, corundum normative basalts through andesites would be widespread in arcs. Although roughly subequal ratios of infiltrating melt:rock, per reaction step, are optimal for producing parental arc magmas, the aggregate melt:rock weight proportions are lower to much lower (ST-6) because the melts react progressively up through the mantle wedge. Under conditions optimal for producing parental arc magmas (infiltrating melt–rock step ratios of 30:70–60:40), melt mass increases several-fold

to as much as tenfold at the maximum melt yield (Fig. 14, ST-6), meaning that a partial melt of subducting basalt in eclogite facies would constitute roughly 1/3 to 1/10 of the final parental magma, diluting high H_2O concentrations to 3–7 wt% at the greatest magma masses (ST-6), consistent with observations from melt inclusions (e.g., summary in Plank et al. 2013). The greatest H_2O concentrations are predicted for the high infiltrating melt:rock ratios that would yield primitive andesites and dacites. Although melt–peridotite reaction can produce such primitive intermediate liquids, the continuity of arc magma compositions from basalts, through andesites and dacites, to rhyodacites and rhyolites (Fig. 15) is strong evidence that mineral-melt differentiation is an overriding control on the compositions of arc magmatic suites.

Rhyolitic melts derived from subducted, dominantly terrigenous sediments would react with peridotite similarly to rhyolitic melts from the basaltic slab, but would have weaker eclogite trace element characteristics due to smaller proportions of residual garnet, more abundant and varied accessory phases, and differences in bulk composition (average global subducted sediment has a modest negative Sr concentration anomaly: Plank and Langmuir 1998).

Conclusions

Melting of hydrous basaltic eclogite is initially peritectic but progresses to eutectic-like in sufficiently hot subducting plates at sub-arc depths. Silicic melts are produced from the H_2O-saturated solidus (± phengite, etc.) to the limit of quartz exhaustion at a piercing point involving quartz, clinopyroxene, and garnet. Beyond quartz exhaustion, melt fraction increases negligibly with temperature due to the thermal steepness of the garnet and clinopyroxene liquidus surfaces that flank the piercing point. This thermal steepness restricts eclogite-facies melts of basaltic sources to rhyolitic (trondhjemitic) compositions at the temperatures predicted for the tops of subducting plates beneath modern magmatic arcs.

Because the piercing-point melts are highly silicic and the liquidus surfaces bounding the piercing point are thermally steep, melt-yield from hydrous basaltic eclogite is mainly limited by the H_2O content and the proportion of quartz in the source. A useful guide is that in present-day, steady-state subduction systems, melt-yields from common sub-alkaline basaltic sources in eclogite facies will not exceed twice the weight fraction of quartz on the solidus. For average spreading-ridge igneous rocks, this restricts melting to no more than about 20 wt%.

Partial melting of hydrous basalt at deep crustal to subcrustal depths, but shallower than eclogite facies, can produce liquids with SiO_2 contents in the range of continental crust and batholiths, but such anatectic liquids are poorer in Mg and have lower Mg# than estimated bulk continental crust and most batholiths. More complex processes, such as mixing of anatectic melts with basalt, reaction of anatectic melts with peridotite, and straightforward crystallization-differentiation from primitive basalts, are likely to be responsible for the elevated Mg concentrations and Mg#s of the continents and batholiths.

Reactions of ascending partial melt of subducting basaltic eclogite with mantle wedge peridotite can produce the major element characteristics of arc basalts through andesites, with the following provisos: magmas that reach the crust in volume typically result from relatively high proportions of infiltrating melt to peridotite (simulated at > 10:90 by reaction step), probably due to channelized flow through the mantle wedge. Primitive andesites and dacites may result from distinctly high proportions of infiltrating melt to peridotite (by step > 50:50). Such magmas are uncommon along modern convergent margins, which may signify that currently subducting plates produce and release partial melts or fluids in lower quantities than early in Earth history. Olivine fractionation has influenced most crustal arc igneous rocks. And, magmas that reach the crust segregate from the mantle wedge at temperatures sufficiently hot to prevent attaining peraluminous compositions near the top of the mantle lithosphere. Reaction between slab melt and peridotite can increase melt mass roughly three- to ten-fold, diluting melt H_2O concentrations to 3–7 wt%, similar to values recorded by melt inclusions.

Reaction between ascending eclogite-facies slab melts and mantle wedge peridotite can also yield the general trace element characteristics of arc magmas and bulk continental crust. Large positive Sr anomalies are predicted for eclogite partial melts, these persist through eclogite melt–peridotite reaction, and they are observed in primitive arc magmas. If such magmas were parental to continental crust, their positive Sr anomalies were largely erased by subsequent crustal-level differentiation that formed plagioclase-bearing cumulates and melting residues with even larger positive Sr anomalies. These cumulates and residues subsequently were removed from arc crust via density instabilities, while buoyant evolved products of magmatic differentiation with smaller to negative Sr anomalies accumulated in the crust. Geochemical variations of representative arc volcanic suites indicate that roughly equal masses of preserved crust and of removed cumulates and melting residues could reduce Sr anomalies to within the range estimated for the bulk continental crust. Subordinate processes may include preferential dissolution of Sr relative to light REE during chemical erosion, and contributions from relamination of subducted sediments with negative Sr anomalies.

Acknowledgements We thank Steve Bohlen and Gary Ernst for their foresight in retaining Jun Liu's run products, starting material, and lab books at the USGS. W. Ben Hankins performed the new 2.6 and 2.8 GPa runs. Jorge Vazquez, Nobu Shimizu, and Karen Hanghøj assisted with ion-microprobe trace element analyses. Robert Oscarson and Leslie Hayden maintained the USGS Menlo Park electron-microprobe facility. Matt Loewen, Gene Yogodzinski, and Dawnika Blatter provided helpful review comments, and Tim Grove and Mike Clynne provided editorial guidance. Any use of trade, firm, or product names is for descriptive purposes only and does not imply endorsement by the U.S. Government.

References

Armstrong JT (1995) CITZAF: a package of correction programs for quantitative electron microbeam X-ray analysis of thick polished materials, thin films, and particles. Microbeam Anal 4:177–200

Bacon CR, Bruggman PE, Christiansen RL, Clynne ME, Donnelly-Nolan JM, Hildreth W (1997) Primitive magmas at five Cascade volcanic fields: melts from hot, heterogeneous sub-arc mantle. Can Miner 35:397–423

Barker F (1979) Trondhjemite: definition, environment, and hypotheses of origin. In: Barker F (ed) Trondhjemites, dacites, and related rocks, developments in petrology 6. Elsevier, Amsterdam, pp 1–11

Behn MD, Kelemen PB, Hirth G, Hacker BR, Massonne H-J (2011) Diapirs as the source of the sediment signature in arc lavas. Nat Geosci 4:641–646

Bista S, Stebbins JF, Hankins WB, Sisson TW (2015) Aluminosilicate melts and glasses at 1 to 3 GPa: temperature and pressure effects on recovered structural and density changes. Am Miner 100:2298–2307

Blackwell DD, Steele JL, Hull DA, Kelley S, Korosec MA (1990) Heat flow in the State of Washington and thermal conditions in the Cascade Range. J Geophys Res 95:19495-19516

Blatter DL, Sisson TW, Hankins WB (2013) Crystallization of oxidized, moderately hydrous basalt at mid- to lower-crustal pressures: implications for andesite genesis. Contrib Miner Pet 166:861–886

Bloch E, Ganguly J, Hervig R, Cheng W (2015) ^{176}Lu-^{176}Hf geochronology of garnet I: experimental determination of the diffusion kinetics of Lu^{3+} and Hf^{4+} in garnet, closure temperatures and geochronological implications. Contrib Miner Pet 169:12. https://doi.org/10.1007/s00410-015-1109-8

Bohlen SR, Boettcher AL (1982) The quartz = coesite transformation: a precise determination and the effects of other components. J Geophys Res 87:7073–7078

Carlson WD (2012) Rates and mechanisms of Y, REE, and Cr diffusion in garnet. Am Mineral 97:1598–1618

Chapman DS (1986) Thermal gradients in the continental crust. In: Dawson JB, Carswell DA, Hall J, Wedepohl KH (eds) The nature of the lower continental crust. Geological Society Special Publications, London, vol 24, pp 63–70

Coleman RG, Lee DE, Beatty LB, Bannock WW (1965) Eclogites and eclogites: their differences and similarities. Geol Soc Am Bull 76:483–508

Cooper LB, Ruscitto DM, Plank T, Wallace PJ, Syracuse EM, Manning CM (2012) Global variations in H_2O/Ce: I. Slab surface temperatures beneath volcanic arcs. Geochem Geophys Geosyst. https://doi.org/10.1029/2011GC003902

Davies JH, Stevenson DJ (1992) Physical model of source region of subduction zone volcanics. J Geophys Res 97:2037–2070

DePaolo DJ (1981) Trace element and isotopic effects of combined wallrock assimilation and fractional crystallization. Earth Planet Sci Lett 53:189–202

Dodge FCW, Moore JG, Papike JJ, Mays RE (1968) Hornblendes from granitic rocks of the central Sierra Nevada batholith California. J Pet 9:378–410

Ernst WG, Liu J (1998) Experimental phase-equilibrium study of Al- and Ti-contents of calcic amphibole in MORB—a semiquantitative thermobarometer. Am Mineral 83:952–969

Furukawa Y (1993) Magmatic processes under arcs and formation of the volcanic front. J Geophys Res 98:8309–8319

Gale A, Dalton CA, Langmuir CH, Su Y, Schilling JG (2013) The mean composition of ocean ridge basalts. Geochem Geophys Geosys 14:489–518

Ghiorso MS, Gualda GAR (2015) An H_2O–CO_2 mixed fluid saturation model compatible with rhyolite-MELTS. Contrib Miner Pet https://doi.org/10.1007/s00410-015-1141-8

Ghiorso MS, Hirschmann MM, Reiners PW, Kress VC (2002) The pMELTS: A revision of MELTS aimed at improving calculation of phase relations and major element partitioning involved in partial melting of the mantle at pressures to 3 GPa. Geochem Geophys Geosys. https://doi.org/10.1029/2001GC000217

Gill JB (1974) Role of underthrust oceanic crust in the genesis of a Fijian calc-alkaline suite. Contrib Mineral Pet 43:29–45

Giordano D, Russell JK, Dingwell DB (2008) Viscosity of magmatic liquids: a model. Earth Planet Sci Lett 271:123–134

Green TH, Ringwood AE (1966) An experimental investigation of the gabbro-eclogite transformation and some geophysical implications. Tectonophys 3:383–427

Green TH, Ringwood AE (1968) Genesis of the calc-alkaline igneous rock suite. Contrib Miner Pet 18:105–162

Grove TL (1993) Corrections to expressions for calculating mineral components in "Origin of calc-alkaline magma lavas at Medicine Lake volcano by fractionation, assimilation, and mixing" and "Experimental petrology of normal MORB near the Kane Fracture Zone: 22–25 N, mid-Atlantic ridge". Contrib Miner Pet 114:422–424

Grove TL, Parman SW, Bowring SA, Price RC, Baker MB (2002) The role of an H_2O-rich fluid component in the generation of primitive basaltic andesites and andesites from the Mt. Shasta region, N California. Contrib Miner Pet 142:375–396

Grove TL, Chatterjee N, Parman SW, Medard E (2006) The influence of H_2O on mantle wedge melting. Earth Planet Sci Lett 249:74–89

Gualda GAR, Ghiorso MS, Lemons RV, Carley TL (2012) Rhyolite-MELTS: a modified calibration optimized for silica-rich, fluid-bearing magmatic systems. J Pet 53:875–890

Hacker BR (2006) Pressures and temperatures of ultrahigh-pressure metamorphism: implications for UHP tectonics and H2O in subducting slabs. Int Geol Rev 48:1053–1066. https://doi.org/10.2747/0020-6814.48.12.1053

Hacker BR, Kelemen PB, Behn MD (2011) Differentiation of the continental crust by relamination. Earth Planet Sci Lett 307:501–516

Hacker BR, Kelemen PB, Behn MD (2015) Continental lower crust. Annu Rev Earth Planet Sci 43:167–205. https://doi.org/10.1146/annurev-earth-050212-124117

Hamilton WB (1969) Mesozoic California and the underflow of the Pacific mantle. Geol Soc Am Bull 80:2409–2430

Hawthorne FC (1981) Crystal chemistry of the amphiboles. In: Veblen DR (ed) Amphiboles and other hydrous pyriboles: mineralogy. Mineralogical Society of America, Washington, DC, vol 9A, pp 1–95

Helz RT (1976) Phase relations of basalts in their melting ranges at P_{H2O}–5 kb. Part II. Melt compositions. J Pet 17:139–193

Hermann J, Rubatto D (2009) Accessory phase control on the trace element signature of sediment melts in subduction zones. Chem Geol 265:512–526

Herzberg C, Asimow PD (2015) PRIMELT3 MEGA.XLSM software for primary magma calculation: peridotite primary magma MgO contents from the liquidus to the solidus. Geochem Geophys Geosyst 16:563–578. https://doi.org/10.1002/2014GC005631

Hill RET, Boettcher AL (1970) Water in the Earth's mantle: Melting curves of basalt-water and basalt-water-carbon dioxide. Science 167:980–982

Jagoutz O, Schmidt MW (2013) The composition of the foundered complement to the continental crust and a re-evaluation of fluxes in arcs. Earth Planet Sci Lett 371–372:177–190

Kay RW (1978) Aleutian magnesian andesites: melts from subducted Pacific Ocean crust. J Volc Geotherm Res 4:117–132

Kelemen PB (1990) Reaction between ultramafic rock and fractionating basaltic magma I. Phase relations, the origin of calc-alkaline magma series, and the formation of discordant dunite. J Pet 31:51–98

Kelemen PB (1995) Genesis of high Mg# andesites and the continental crust. Contrib Miner Pet 120:1–19

Kelemen PB, Behn MD (2016) Formation of lower continental crust by relamination of buoyant arc lavas and plutons. Nature Geosci 9:197–205

Kelemen PB, Hanghoj K, Greene AR (2003a) One view of the geochemistry of subduction-related magmatic arcs, with an emphasis on primitive andesite and lower crust. In: Holland HD, Turekian KK (eds) Treatise on geochemistry, vol 3, pp 593–659

Kelemen PB, Parmentier EM, Rilling J, Mehl L, Hacker BR (2003b) Thermal structure due to solid-state flow in the mantle wedge beneath arcs. In: Eiler J (ed) Inside the subduction factory. American Geophysical Union Geophysical Monograph, Washington DC, vol 138, pp 293–311

Kelemen PB, Yogodzinski GM, Scholl DW (2003c) Along-strike variation in the Aleutian Island arc: genesis of high Mg# andesite and implications for continental crust. In: Eiler J (ed) Inside the subduction factory. American Geophysical Union Geophysical Monograph Series, Washington DC, vol 138, pp 223–276

Kelemen PB, Hanghoj K, Greene AR (2014) One view of the geochemistry of subduction-related magmatic arcs, with an emphasis on primitive andesite and lower crust. In: Holland HD, Turekian KK (eds) Treatise on geochemistry, vol 3, pp 1–70. https://doi.org/10.1016/B978-0-08-095975-7.00323-5

Kessel R, Schmidt MW, Ulmer P, Pettke T (2005a) Trace element signature of subduction-zone fluids, melts, and supercritical liquids at 120–180 km depth. Nature 437:724–727

Kessel R, Ulmer P, Pettke T, Schmidt MW, Thompson AB (2005b) The water-basalt system at 4 to 6 GPa: Phase relations and second critical endpoint in a K-free eclogite at 700 to 1400 °C. Earth Planet Sci Lett 237:873–892

Klemme S, Blundy JD, Wood BJ (2002) Experimental constraints on major and trace element partitioning during partial melting of eclogite. Geochim Cosmochim Acta 66:3109–3123

Klimm K, Blundy JD, Green TH (2008) Trace element partitioning and accessory phase saturation during H_2O-saturated melting of basalt with implications for subduction zone chemical fluxes. J Pet 49:523–553

Lambert IB, Wyllie PJ (1972) Melting of gabbro (quartz eclogite) with excess water to 35 kilobars, with geological applications. J Geol 80:693–708

Lehnert K, Su Y, Langmuir C, Sarbas B, Nohl U (2000) A global geochemical database structure for rocks. Geochem Geophys Geosys. https://doi.org/10.1029/1999GC000026

Liu J (1997) High pressure phase equilibria involving the amphibolite-eclogite transformation. PhD dissertation, Stanford University, Stanford, California

Liu J, Bohlen SR (1995) Mixing properties and stability of jadeite–acmite pyroxene in the presence of albite and quartz. Contrib Miner Pet 119:433–440

Liu J, Bohlen SR, Ernst WG (1996) Stability of hydrous phases in subducting oceanic crust. Earth Planet Sci Lett 143:161–171

Macdonald R, Smith RL, Thomas JE (1992) Chemistry of the subalkalic obsidians. US Geol Surv Prof Pap 1523:214 pp

Martin H (1986) The effect of steeper Archean geothermal gradient on the geochemistry of subduction-zone magmas. Geology 14:753–756

Martin H, Smithies RH, Rapp R, Moyen J-F, Champion D (2005) An overview of adakite, tonalite-trondhjemite-granite (TTG), and sanukitoid: relationships and some implications for crustal evolution. Lithos 79:1–24

McDonough WF, Sun S-S (1995) Composition of the earth. Chem Geol 120:223–253

Miyashiro A (1974) Volcanic rock series in island arcs and active continental margins. Am J Sci 274:321–355

Mooney WD, Kaban MK (2010) The North American upper mantle: density, composition, and evolution. J Geophys Res 115:B12424. https://doi.org/10.1029/2010JB000866

Morgan GB, London D (1996) Optimizing the electron microbeam analysis of alkali aluminosilicate glasses. Am Miner 81:1176–1185

Morimoto N (1988) Nomenclature of pyroxenes. Miner Pet 39:55–76

Peacock SM (1990) Numerical simulation of metamorphic pressure-temperature-time paths and fluid production in subducting slabs. Tectonophys 9:1197–1211

Peacock SM, van Keken PE, Holloway SD, Hacker BR, Abers GA, Fergason RL (2005) Thermal structure of the Costa Rica–Nicaragua subduction zone. Phys Earth Planet Inter 149:187–200

Penniston-Dorland SC, Kohn MJ, Manning CE (2015) The global range of subduction zone thermal structures from exhumed blueschists and eclogites: rocks are hotter than models. Earth Planet Sci Lett 428:243–254

Perfit MR, Gust DA, Bence AE, Arculus RJ, Taylor SR (1980) Chemical characteristics of island-arc basalts: implications for mantle sources. Chem Geol 30:227–256

Pertermann M, Hirschmann MM (2003) Partial melting experiments on a MORB-like pyroxenite between 2 and 3 GPa: constraints on the presence of pyroxenite in basalt source regions from solidus location and melting rate. J Geophys Res. https://doi.org/10.1029/2000JB000118

Pichavant M, Valencia Herrera J, Boulmier S, Briqueu L, Joron J-L, Juteau M, Marin L, Michard A, Sheppard SMF, Treuil M, Vernet M (1987) The Macusani glasses, SE Peru: evidence of chemical fractionation in peraluminous magmas. In: Mysen BO (ed) Magmatic processes: physicochemical principles. Geochemical Society Special Publications, Washington, DC, vol 1, pp 359–373

Plank T (2005) Constraints from thorium/lanthanum on sediment recycling at subduction zones and the evolution of the continents. J Pet 46:921–944

Plank T, Langmuir CH (1998) The chemical composition of subducting sediment and its consequences for the crust and mantle. Chem Geol 145:325–394

Plank T, Cooper LB, Manning CE (2009) Emerging geothermometers for estimating slab surface temperatures. Nature Geosci 2:611–615

Plank T, Kelley KA, Zimmer MM, Hauri EH, Wallace PJ (2013) Why do mafic arc magmas contain~ 4 wt% water on average? Earth Planet Sci Lett 364:168–179

Poli S, Schmidt MW (2002) Petrology of subducted slabs. Ann Rev Earth Planet Sci 30:207–237

Pollack HN, Hurter SJ, Johnson JR (1993) Heat flow from the Earth's interior: analysis of the global data set. Rev Geophys 31:267–280

Rapp RP (1995) Amphibole-out boundary in partially melted metabasalt, its control over liquid fraction and composition, and source permeability. J Geophys Res 100:15601–15610

Rapp RP, Watson EB (1995) Dehydration-melting of metabasalt at 8–32 kbar: Implications for continental growth and crust-mantle recycling. J Pet 36:891–931

Rapp RP, Watson EB, Miller CF (1991) Partial melting of amphibolite/eclogite and the origin of Archean trondhjemites and tonalities. Precamb Res 51:1–25

Ratajeski K (1999) Field, geochemical, and experimental study of mafic to felsic plutonic rocks associated with the intrusive suite of Yosemite Valley, California. PhD thesis, University of North Carolina, Chapel Hill, pp 196

Ringwood AE (1977) Petrogenesis in island arc systems. In: Talwani M, Pitman WC (eds) Island arcs, deep sea trenches and backarc basins. Maurice Ewing Series I. American Geophysical Union, Washington DC, pp 311–324

Ringwood AE, Green DH (1966) An experimental investigation of the gabbro-eclogite transformation and some geophysical implications. Tectonophys 3:383–427

Rudnick RL, Gao S (2003) Composition of the continental crust. Treatise Geochem 3:1–64

Rushmer T (1991) Partial melting of two amphibolites: contrasting experimental results under fluid-absent conditions. Contrib Miner Pet 107:41–59

Schmidt MW, Poli S (1998) Experimentally based water budgets for dehydrating slabs and consequences for arc magma generation. Earth Planet Sci Lett 163:361–379

Schmidt MW, Vielzeuf D, Auzanneau E (2004) Melting and dissolution of subducting crust at high pressures: the key role of white mica. Earth Planet Sci Lett 228:65–84

Shaw DM (2000) Continuous (dynamic) melting theory revisited. Can Miner 38:10411063

Shimizu N, Hart SR (1982) Applications of the ion microprobe to geochemistry and cosmochemistry. Ann Rev Earth Planet Sci 10:483–526

Sisson TW, Ratajeski K, Hankin WB, Glazner AF (2005) Voluminous granitic magmas from common basaltic sources. Contrib Miner Pet 148:635–661

Skjerlie KP, Patiño Douce AE (2002) The fluid absent partial melting of a zoisite-bearing quartz eclogite from 1.0 to 3.2 GPa; implications for melting in thickened continental crust and for subduction-zone processes. J Pet 43:291–314

Skora S, Blundy J (2012) Monazite solubility in hydrous silicic melts at high pressure conditions relevant to subduction zone metamorphism. Earth Planet Sci Lett 321–322:104–114

Sleep NH, Windley BF (1982) Archean plate tectonics: constraints and inferences. J Geol 90:363–379

Stolper E, Newman S (1994) The role of water in the petrogenesis of Mariana trough magmas. Earth Planet Sci Lett 121:293–325

Streckeisen A (1976) To each plutonic rock its proper name. Earth Sci Rev 12:1–33

Syracuse EM, van Keken PE, Abers GA (2010) The global range of subduction zone thermal models. Phys Earth Planet Inter 183:73–90

Tang M, Rudnick RL, McDonough WF, Gaschnig RM, Huang Y (2015) Europium anomalies constrain the mass of recycled lower continental crust. Geol 43:703–706

Taylor SR, McLennan SM (1985) The continental crust: its composition and evolution. Blackwell Sci Pubs, Oxford, p 312

Till CB, Grove TL, Withers AC (2012) The beginnings of hydrous mantle wedge melting. Contrib Miner Pet 163:669–688

Tirone M, Ganguly J, Dohmen R, Langenhorst F, Hervig R, Becker H-W (2005) Rare earth diffusion kinetics in garnet: experimental studies and applications. Geochim Cosmochim Acta 69:2385–2398

Ulmer P, Trommsdorff (1995) Serpentine stability to mantle depths and subduction-related magmatism. Science 268:858–861

van Keken PE, Kiefer B, Peacock SM (2002) High-resolution models of subduction zones: Implications for mineral dehydration reactions and the transport of water into the deep mantle. Geochem Geophys Geosys 3:1056. https://doi.org/10.1029/2001GC000256

Wada I, Wang K (2009) Common depth of slab-mantle decoupling: Reconciling diversity and uniformity of subduction zones. Geochem Geophys Geosyst 10:Q10009. https://doi.org/10.1029/2009GC002570

Winther KT (1996) An experimentally based model for the origin of tonalitic and trondhjemitic melts. Chem Geol 127:43–59

Wolf MB, Wyllie PJ (1994) Dehydration-melting of amphibolite at 10 kbar: the effects of temperature and time. Contrib Miner Pet 115:369–383

Workman RK, Hart SR (2005) Major and trace element composition of the depleted MORB mantle (DMM). Earth Planet Sci Lett 231:53–72

Wyllie PJ (1973) Experimental petrology and global tectonics: a preview. Tectonophysics 17:189–209

Yoder HS Jr, Tilley CE (1962) Origin of basalt magmas: an experimental study of natural and synthetic rock systems. J Pet 3:342–532

Yogodzinski GM, Kay RW, Volynets ON, Koloskov AV, Kay SM (1995) Magnesian andesite in the western Aleutian Komondorsky region: Implications for slab melting and processes in the mantle wedge. Geol Soc Am Bull 107:505–519